Electronic Supplementary Material (ESI) for Journal of Materials Chemistry A.
This journal is © The Royal Society of Chemistry 2018

Supplementary Information

Exploring Polycyclic Aromatic Hydrocarbons as Anolyte for Nonaqueous Redox Flow Batteries

Gongwei Wang[1], Bing Huang[2], Dan Liu[1], Dong Zheng[1], Joshua Harris[1], Janie Xue[1], Deyang Qu[1*]

[1]*Department of Mechanical Engineering, College of Engineering and Applied Science, University of Wisconsin Milwaukee, Milwaukee, WI 53211, USA.* *E-mail: qud@uwm.edu*

[2]*Institute of Physical Chemistry and National Center for Computational Design and Discovery of Novel Materials (MARVEL), Department of Chemistry, University of Basel, Klingelbergstrasse 80, 4056 Basel, Switzerland*

1. Choosing the supporting electrolyte and solvent

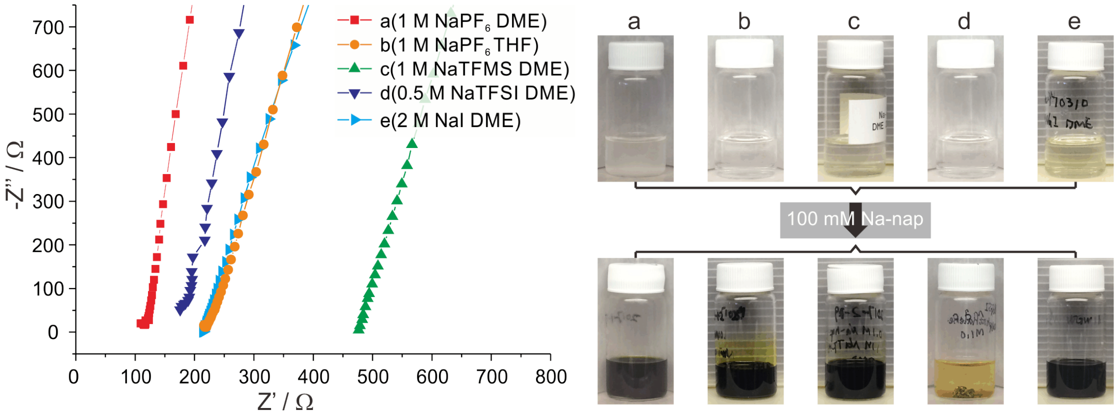

Fig. S1. Electrochemical impedance spectra (EIS) of different blank electrolytes (left). Photographs of blank electrolytes before and after adding Nap together with Na metal (right). It seems that $Nap^{\bullet-}$ cannot form in 0.5 M NaTFSI / DME solution, which could be induced by the passivation of Na metal surface and thus forbid the reaction between Na and Na metal.

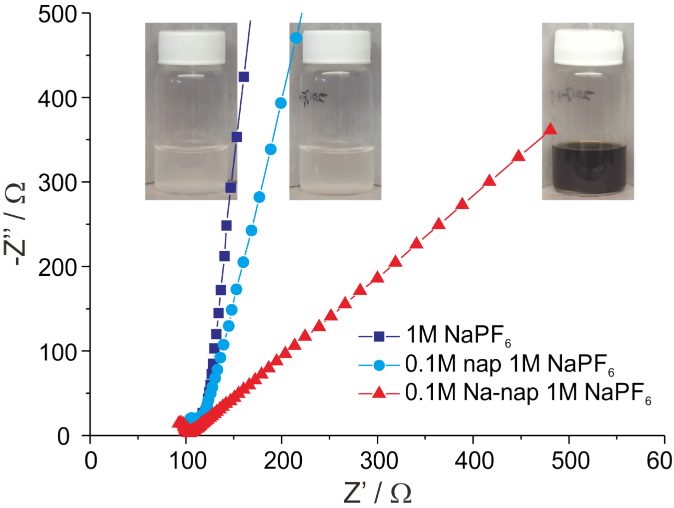

Fig. S2. Electrochemical impedance spectra (EIS) and photographs of blank electrolyte (1 M NaPF$_6$ / DME), 0.1 M Nap contained electrolyte and 0.1 M Na-Nap contained electrolyte.

2. Determination of the concentration of redox-active species

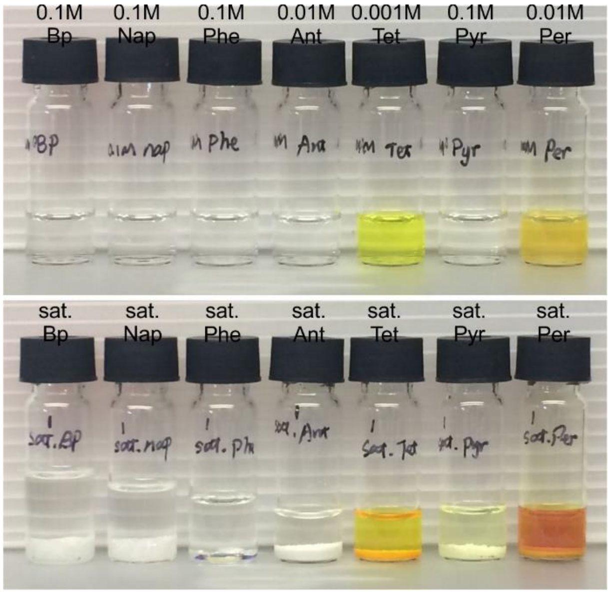

Fig. S3. Photographs of unsaturated (upper) and saturated (lower) PAH (PAH = Bp, Nap, Phe, Ant, Tet, Pyr, Per) DME solutions. The solution volume increased significantly when preparing saturated Bp, Nap and Phe solutions. Therefore, it's difficult to determine the saturated concentration just by the amount of solute added into the solution until the appearance of precipitation.

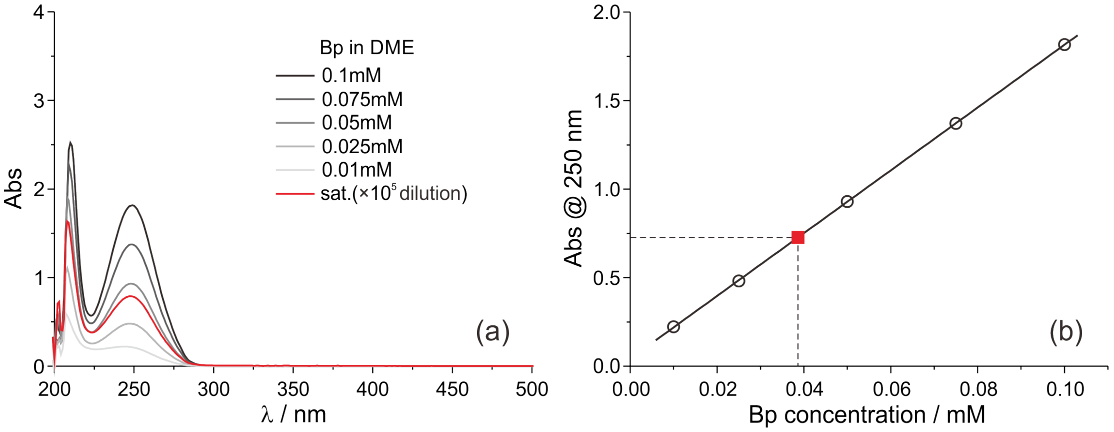

Fig. S4. UV-vis spectra (a) and calibration curve (b) of Bp in DME solution

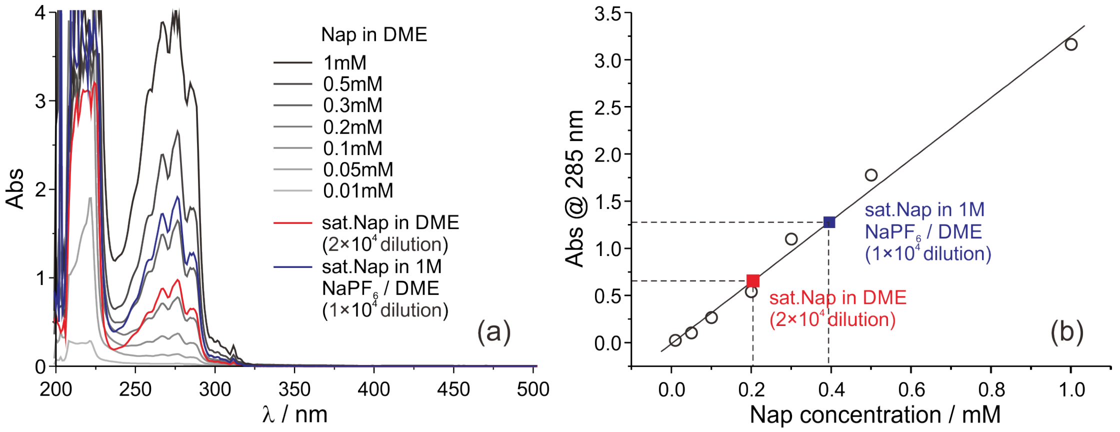

Fig. S5. UV-vis spectra (a) and calibration curve (b) of Nap in DME solution. The solubility of Nap in 1 M $NaPF_6$ / DME (3.95 M) is slightly lower than that of in DME (4.04 M).

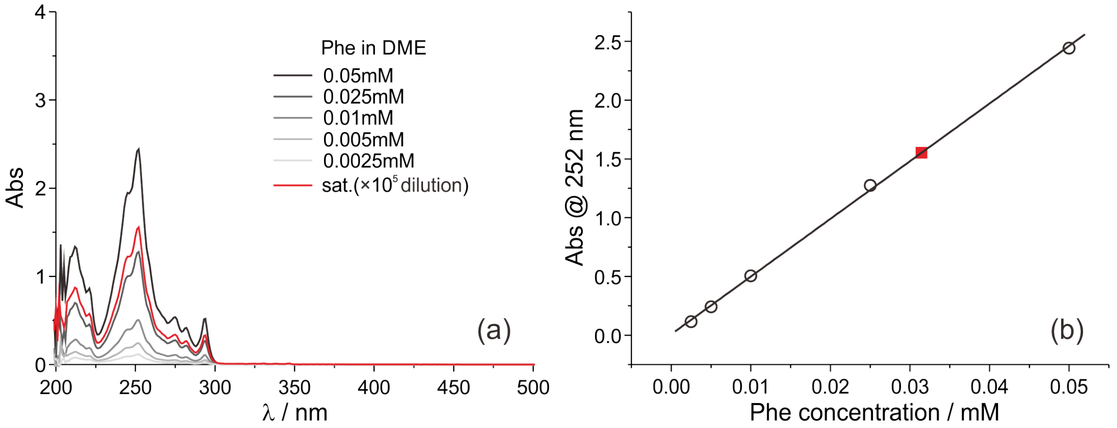

Fig. S6. UV-vis spectra (a) and calibration curve (b) of Phe in DME solution

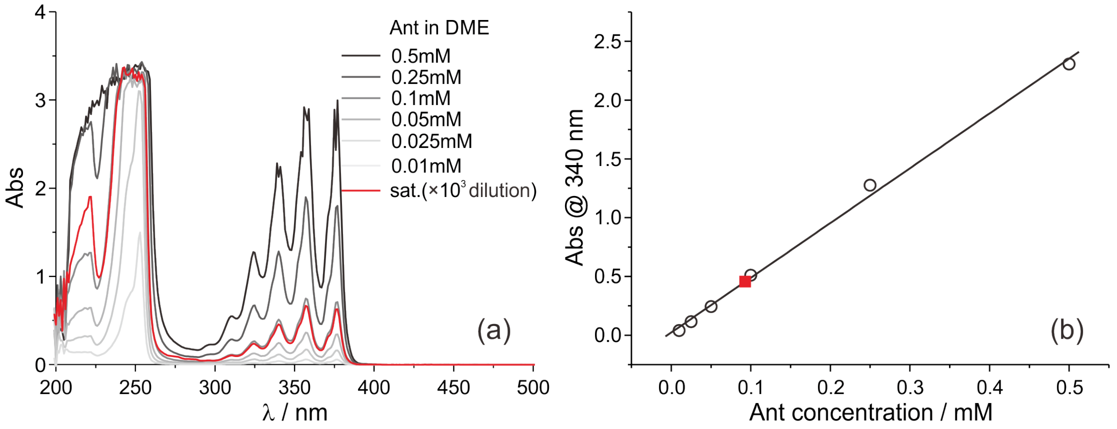

Fig. S7. UV-vis spectra (a) and calibration curve (b) of Ant in DME solution

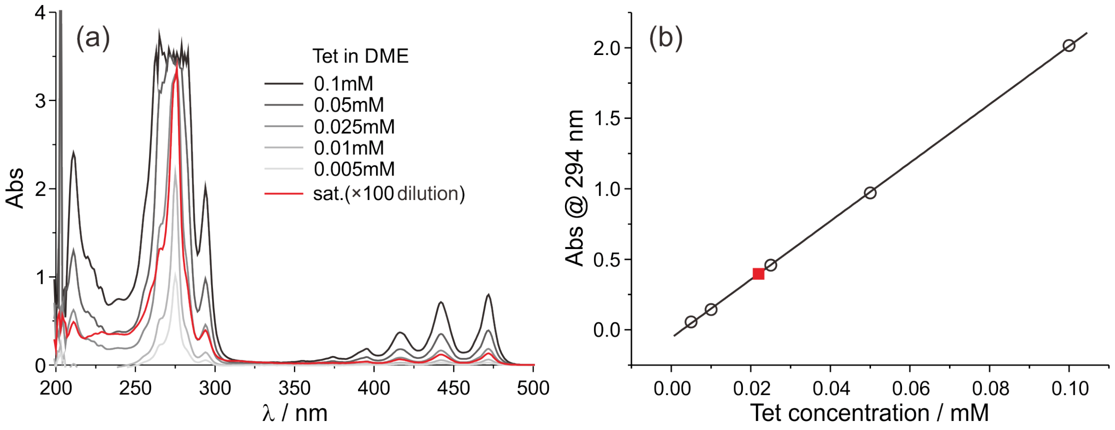

Fig. S8. UV-vis spectra (a) and calibration curve (b) of Tet in DME solution

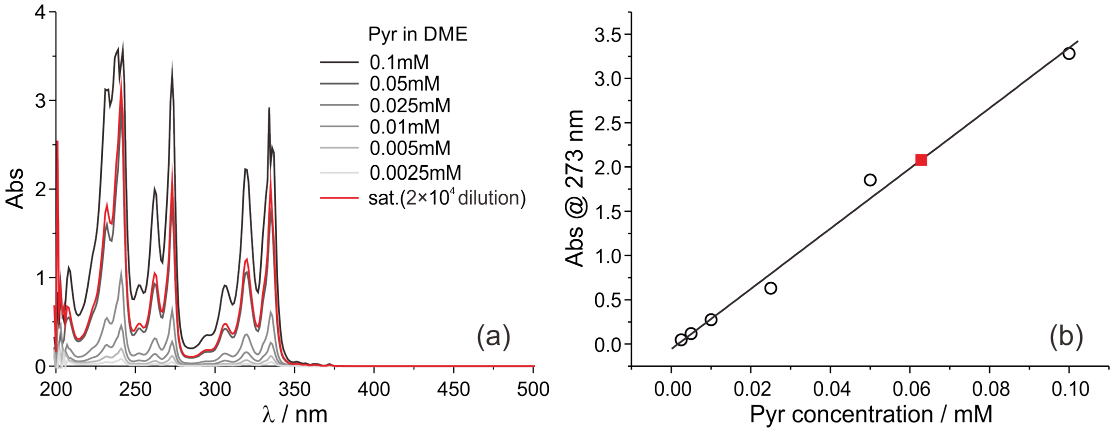

Fig. S9. UV-vis spectra (a) and calibration curve (b) of Pyr in DME solution

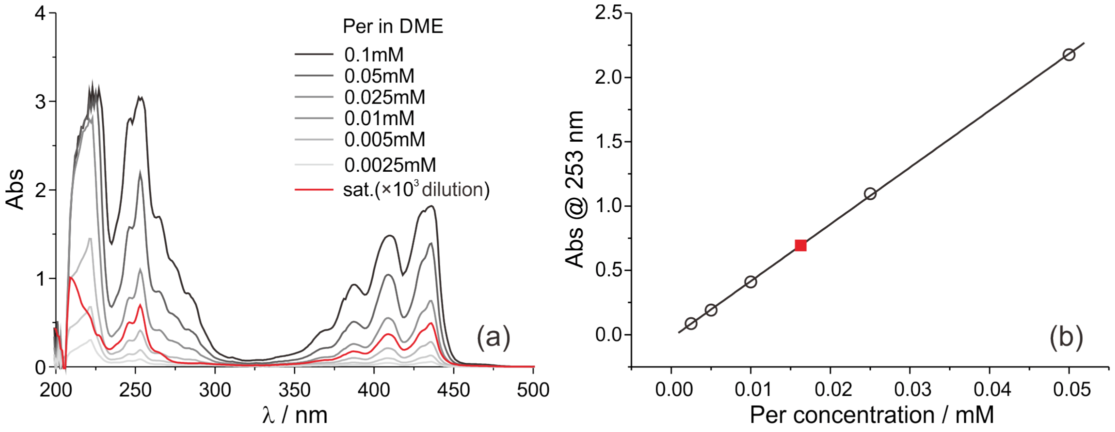

Fig. S10. UV-vis spectra (a) and calibration curve (b) of Per in DME solution

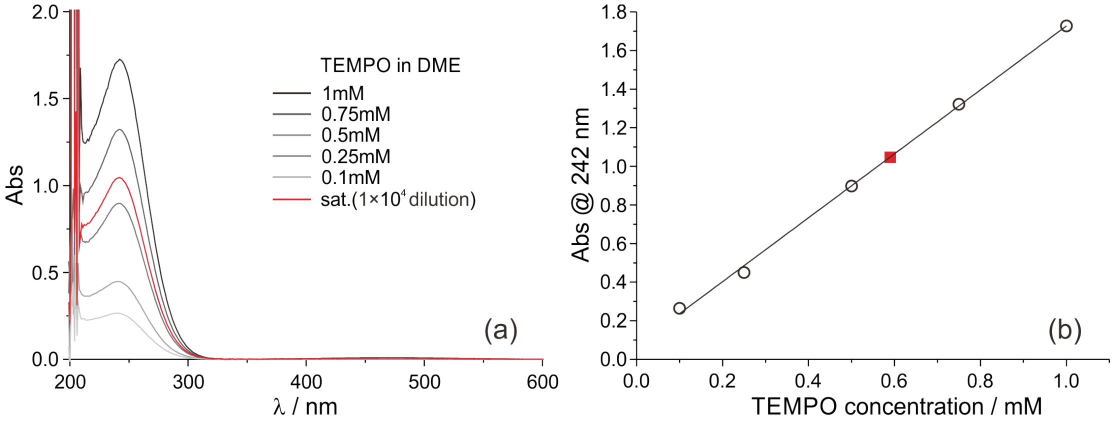

Fig. S11. UV-vis spectra (a) and calibration curve (b) of TEMPO in DME solution

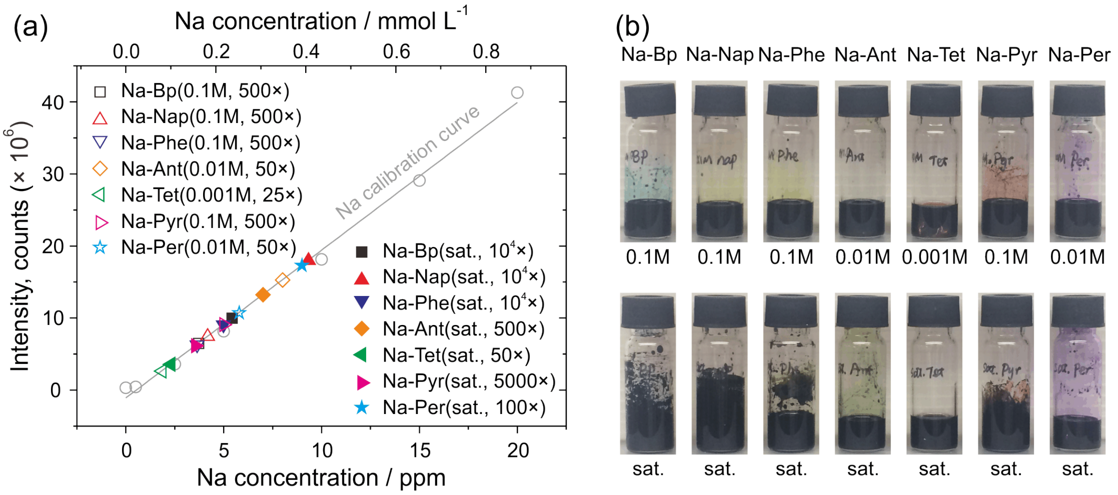

Fig. S12. (a) The concentrations of Na (*c*(Na) in Na-PAH contained DME solutions determined by ICP calibration curve method. (b) Photographs of Na-PAH contained DME solutions with given and saturated concentrations.

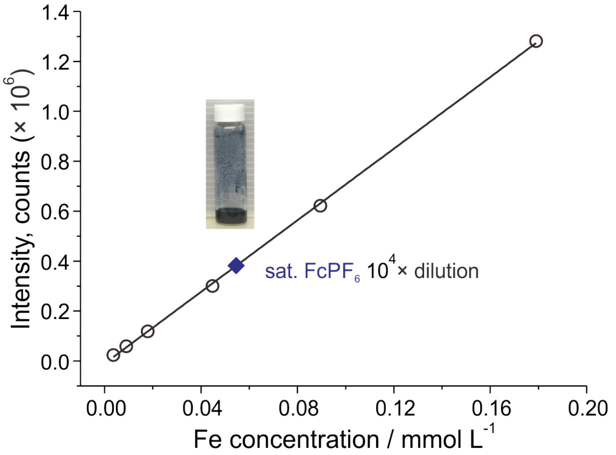

Fig. S13. Saturated concentration of $FcPF_6$ in 1M $NaPF_6$ / DME determined by ICP calibration curve method. Insert is the photograph of $FcPF_6$ saturated 1M $NaPF_6$ / DME solution.

Table S1. A summary of the saturated concentrations of redox species determined by UV-vis or ICP analysis.

Redox species	Unsaturated solution			Saturated solution		
	c(PAH) / M	*c*(Na) / M	*c*(Na)/*c*(PAH)	*c*(PAH) / M	*c*(Na) / M	*c*(Na)/*c*(PAH)
Bp	0.1	0.0809	0.81	3.9	2.3615	0.61
Nap	0.1	0.0910	0.91	4	4.0585	1.01
Phe	0.1	0.0791	0.79	3.145	2.1688	0.69
Ant	0.01	0.0174	1.74	0.093	0.1525	1.64
Tet	0.001	0.0020	2.02	0.002196	0.005009	2.28
Pyr	0.1	0.1087	1.09	1.2572	0.7742	0.62
Per	0.01	0.0196	1.97	0.01628	0.02521	1.55
				c / M		
$FcPF_6$				0.55		
TEMPO				5.9		

4. Electrochemical performance of PAH / $\text{PAH}^{\bullet n-}$ redox species

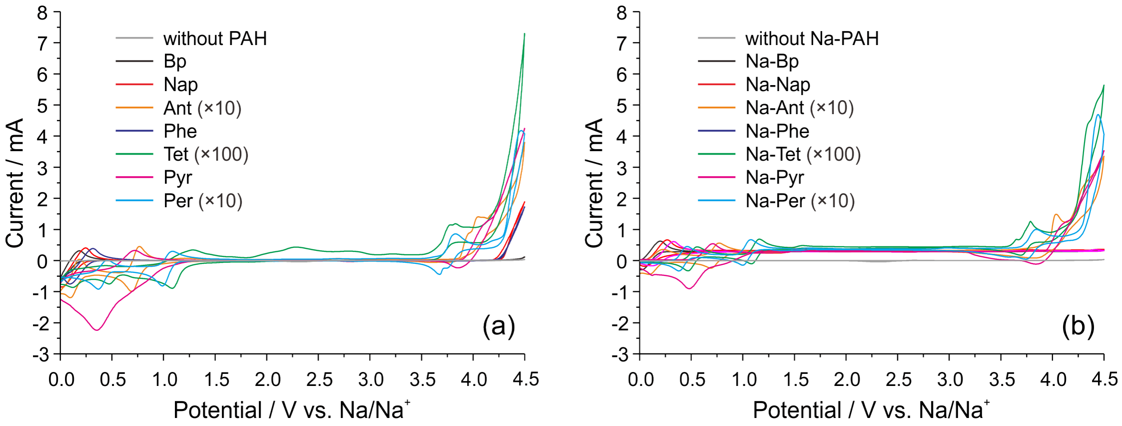

Fig. S14. CV curves for PAH (a) and Na-PAH (b) contained electrolytes at the potential range from 0 V to 4.5 V (vs. Na/Na^+) and a scan rate of 20 mV/s. PAH = 0.1 M Bp, 0.1 M Nap, 0.1 M Phe, 0.01 M Ant, 0.001 M Tet, 0.1 M Pyr and 0.01 M Per; Na-PAH = 0.1 M Na-Bp, 0.1 M Na-Nap, 0.1 M Na-Phe, 0.01 M Na-Ant, 0.001 M Na-Tet, 0.1 M Na-Pyr and 0.01 M Na-Per. For CV curves in Pyr or Na-Pyr contained electrolytes, the reduction current below 1.5 V (vs. Na/Na^+) was much larger compared with other systems owing to the electrochemical polymerization of Pyr as reported by Bachman et al. (*Nat. Commun.* **2015**, *6*, 7040). The resulting polymer films were clearly observed after several CV cycles (Fig. S15).

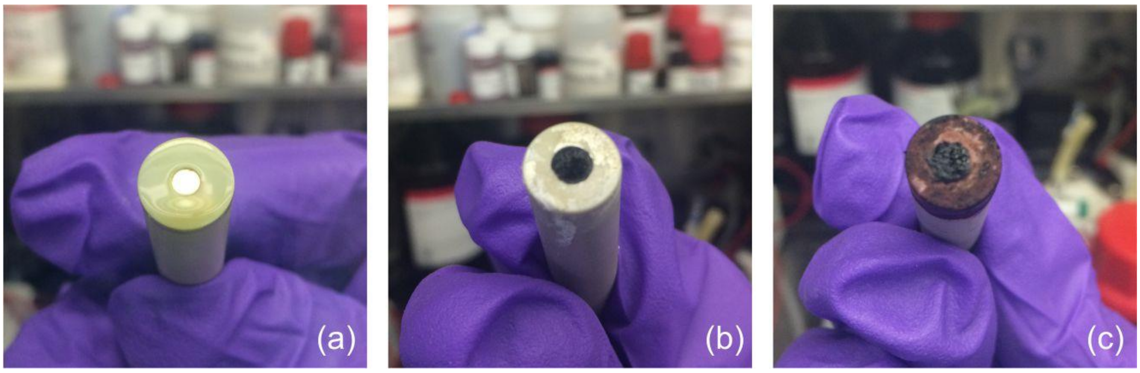

Fig. S15. Photographs of Pt RDE before (a) and after CV measurement (with an upper potential limit of 4.5 V vs. Na/Na$^+$) in Pyr contained electrolyte (b) or Na-Pyr contained electrolyte (c). A polymer film formed onto the surface of Pt RDE was clearly observed after several CV cycles.

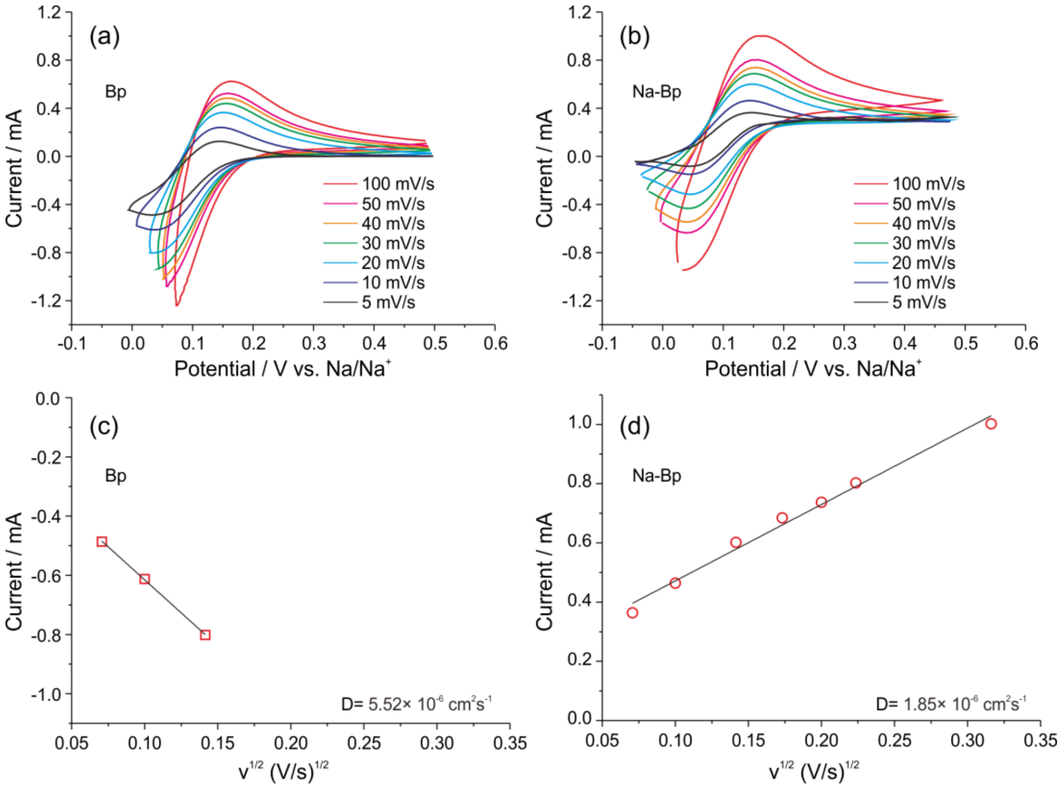

Fig. S16. *i*R-corrected CV curves for 0.1 M Bp (a) and 0.1 M Na-Bp (b) contained electrolytes at different scan rates. linear relationship between i_p and $v^{1/2}$ obtained from CV curves (c, d).

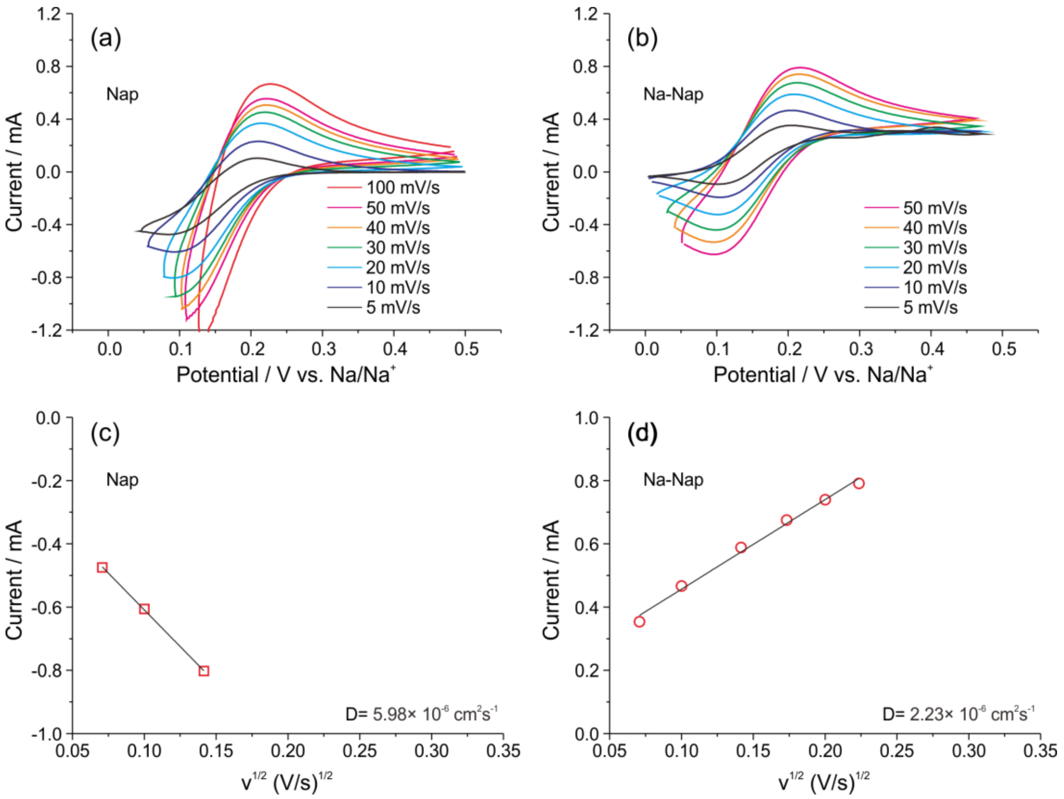

Fig. S17. *i*R-corrected CV curves for 0.1 M Nap (a) and 0.1 M Na-Nap (b) contained electrolytes at different scan rates. linear relationship between i_p and $v^{1/2}$ obtained from CV curves (c, d).

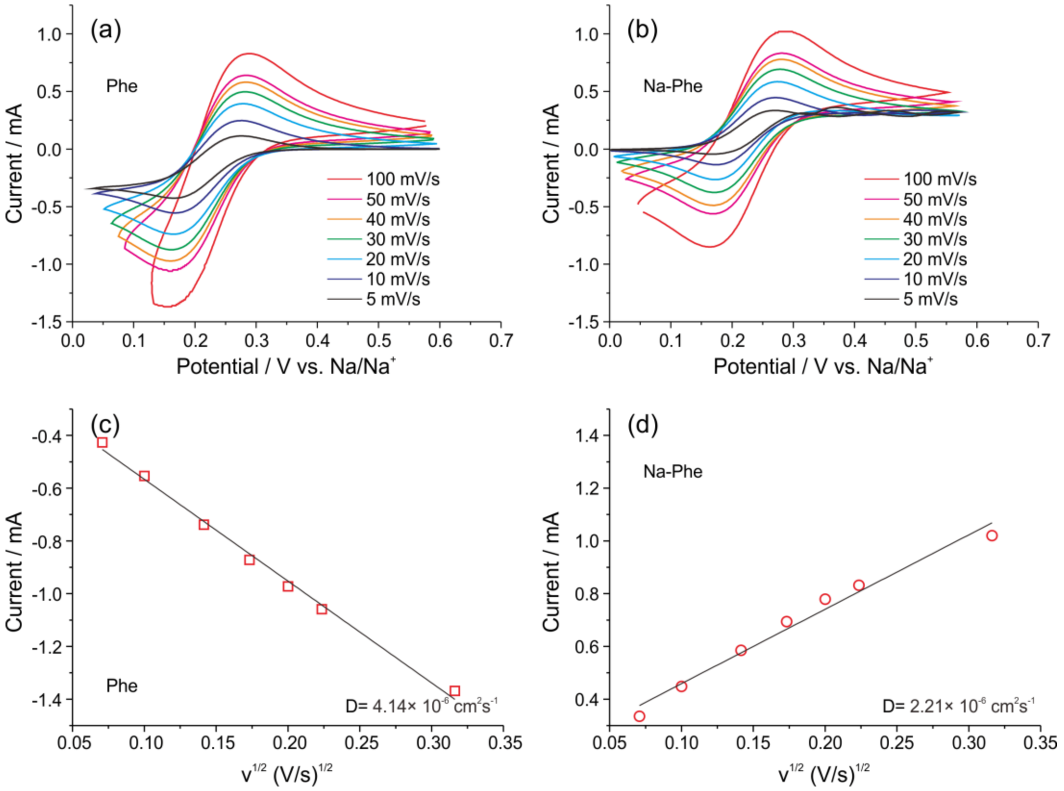

Fig. S18. *i*R-corrected CV curves for 0.1 M Phe (a) and 0.1 M Na-Phe (b) contained electrolytes at different scan rates. linear relationship between i_p and $v^{1/2}$ obtained from CV curves (c, d).

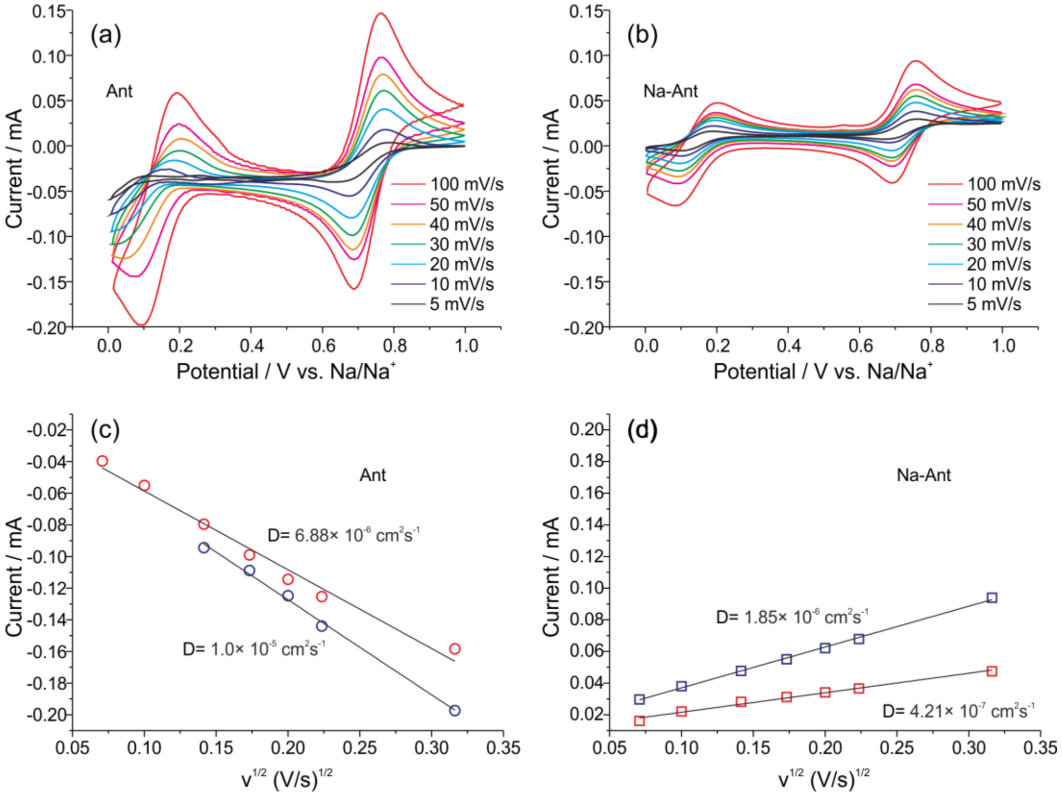

Fig. S19. *i*R-corrected CV curves for 0.01 M Ant (a) and 0.01 M Na-Ant (b) contained electrolytes at different scan rates. linear relationship between i_p and $v^{1/2}$ obtained from CV curves (c, d).

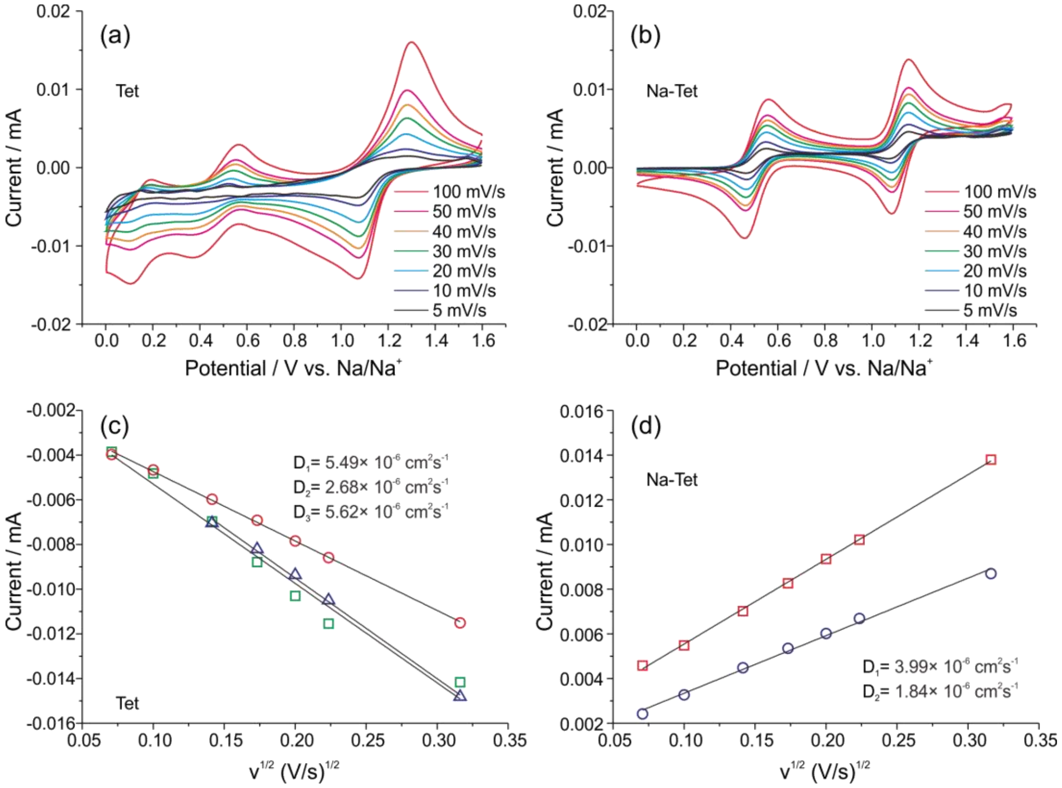

Fig. S20. *i*R-corrected CV curves for 0.001 M Tet (a) and 0.001 M Na-Tet (b) contained electrolytes at different scan rates. linear relationship between i_p and $v^{1/2}$ obtained from CV curves (c, d).

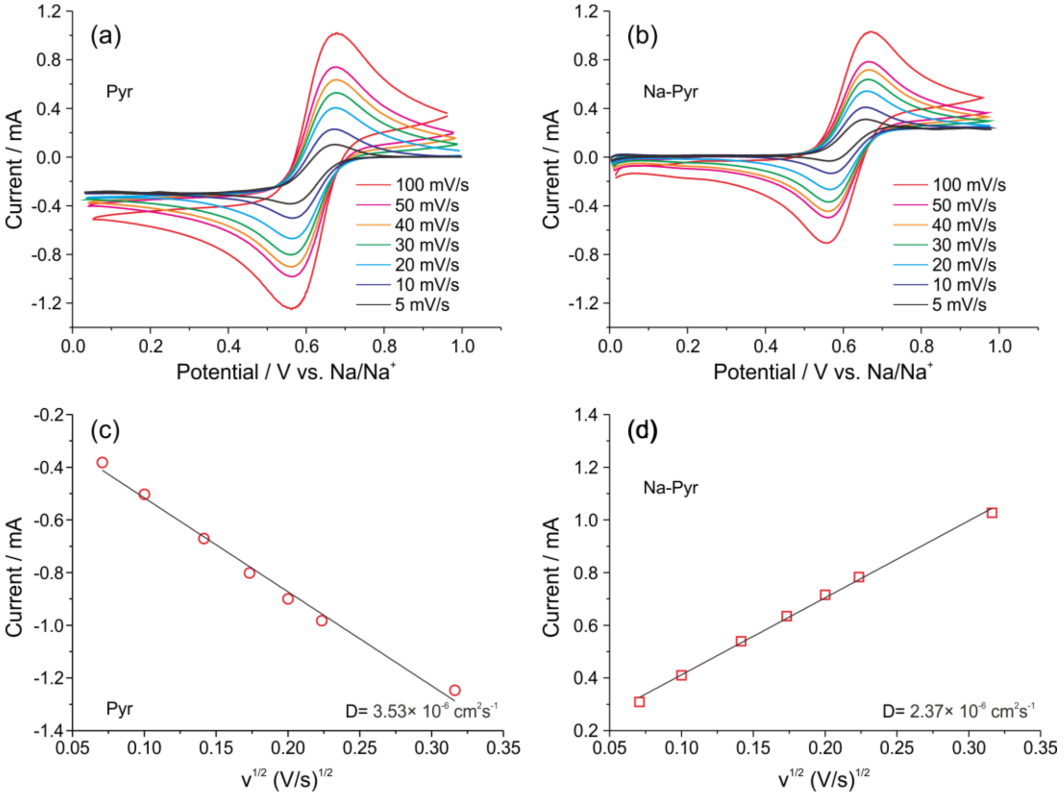

Fig. S21. *i*R-corrected CV curves for 0.1 M Pyr (a) and 0.1 M Na-Pyr (b) contained electrolytes at different scan rates. linear relationship between i_p and $v^{1/2}$ obtained from CV curves (c, d).

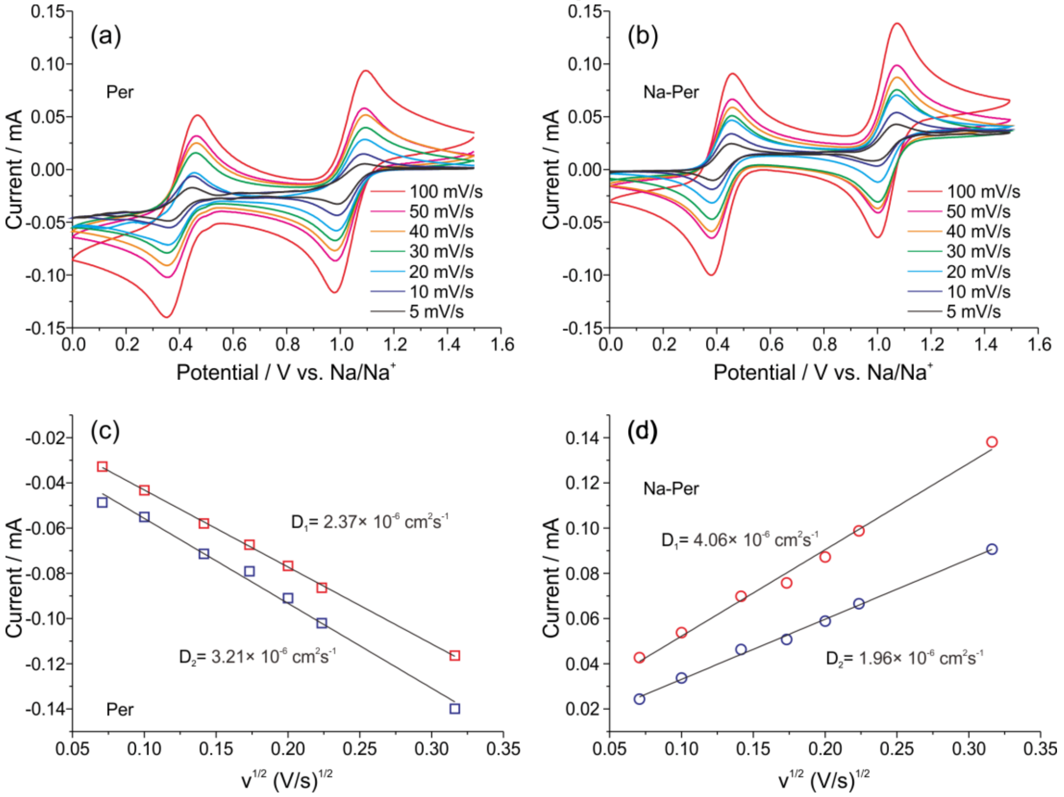

Fig. S22. *i*R-corrected CV curves for 0.01 M Per (a) and 0.01 M Na-Per (b) contained electrolytes at different scan rates. linear relationship between i_p and $v^{1/2}$ obtained from CV curves (c, d).

Table S2. The diffusion coefficient (*D*, cm^2/s) calculated by the Randle-Sevcik equation.

	D, ×10^{-6} cm^2/s				*D*, ×10^{-6} cm^2/s		
	PAH	PAH$^{\bullet-}$	PAH$^{\bullet 2-}$		PAH$^{\bullet-}$	PAH$^{\bullet 2-}$	PAH$^{\bullet 3-}$
Bp	5.52			Na-Bp	1.85		
Nap	5.98			Na-Nap	2.23		
Phe	4.14			Na-Phe	2.21		
Ant	6.88	10.0		Na-Ant	1.85	0.42	
Tet	5.49	2.68	5.62	Na-Tet	3.99	1.84	
Pyr	3.53			Na-Pyr	2.37		
Per	3.21	3.91		Na-Per	4.06	1.96	

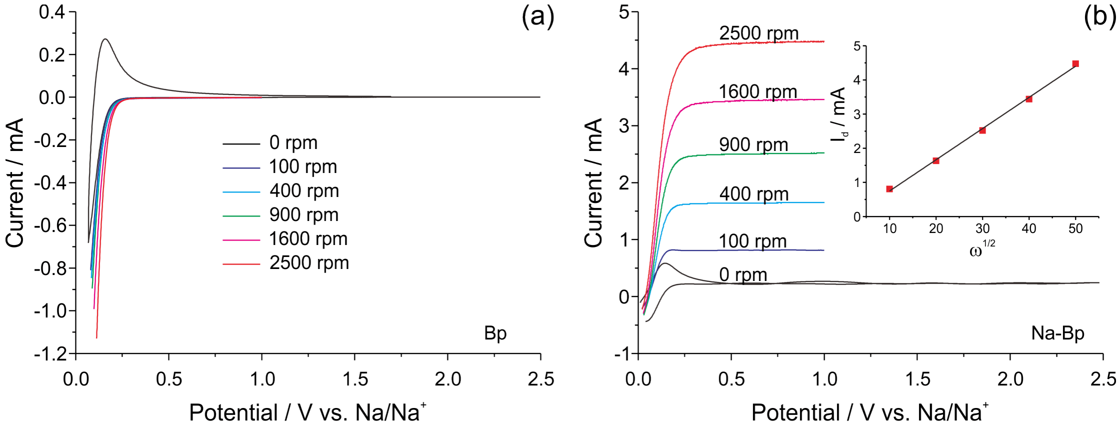

Fig. S23. *i*R-corrected LSV curves for 0.1 M Bp (a) and 0.1 M Na-Bp (b) contained electrolytes at various rotation speeds. Insert is the Levich plot of diffusion-limited current (i_d) vs. square root of rotation ($\omega^{1/2}$).

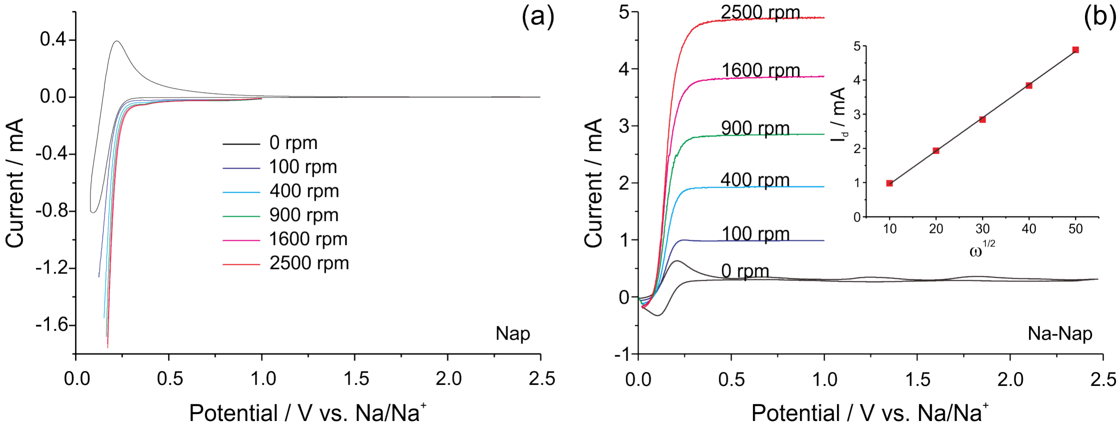

Fig. S24. *i*R-corrected LSV curves for 0.1 M Nap (a) and 0.1 M Na-Nap (b) contained electrolytes at various rotation speeds. Insert is the Levich plot of diffusion-limited current (i_d) vs. square root of rotation ($\omega^{1/2}$).

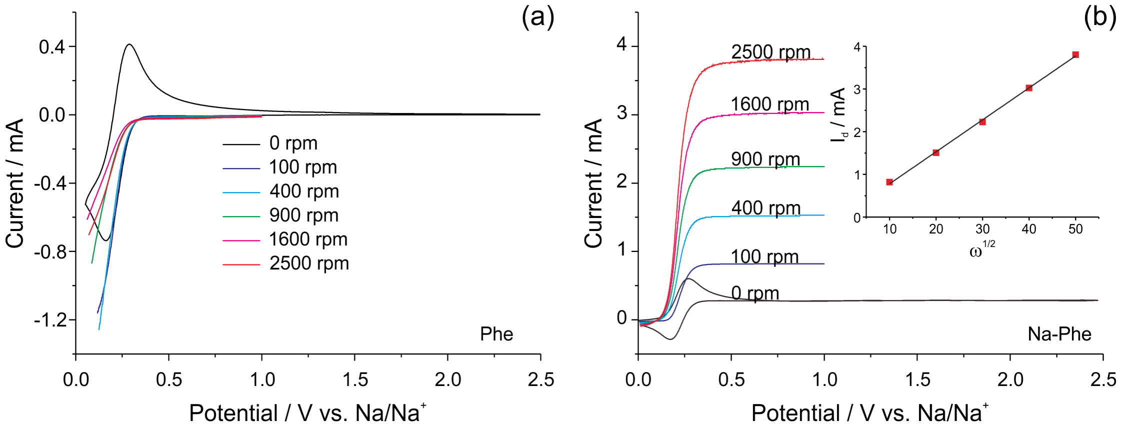

Fig. S25. *i*R-corrected LSV curves for 0.1 M Phe (a) and 0.1 M Na-Phe (b) contained electrolytes at various rotation speeds. Insert is the Levich plot of diffusion-limited current (i_d) vs. square root of rotation ($\omega^{1/2}$).

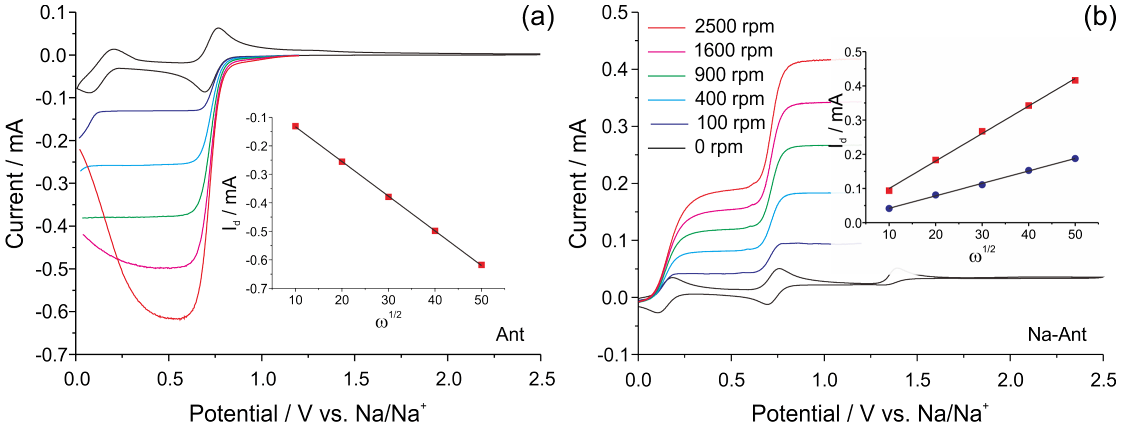

Fig. S26. *i*R-corrected LSV curves for 0.01 M Ant (a) and 0.01 M Na-Ant (b) contained electrolytes at various rotation speeds. Insert are the Levich plots of diffusion-limited current (i_d) vs. square root of rotation ($\omega^{1/2}$).

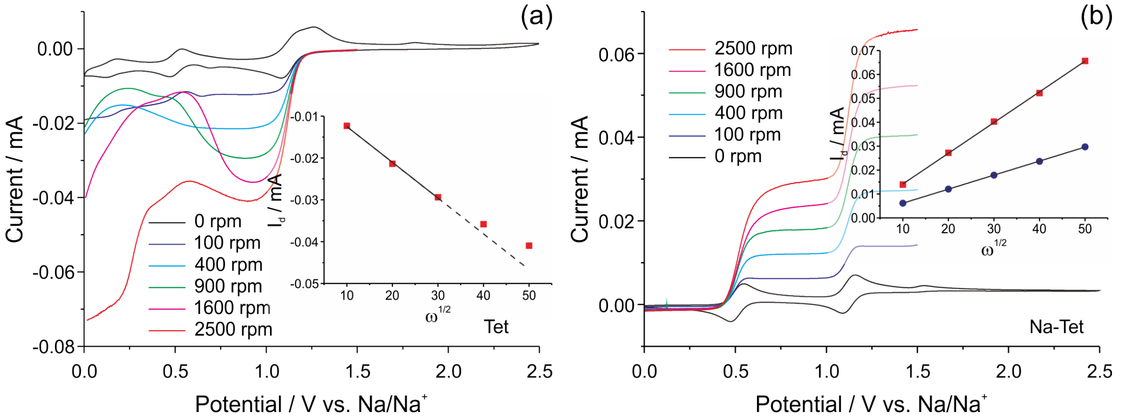

Fig. S27. *i*R-corrected LSV curves for 0.001 M Tet (a) and 0.001 M Na-Tet (b) contained electrolytes at various rotation speeds. Insert are the Levich plots of diffusion-limited current (i_d) vs. square root of rotation ($\omega^{1/2}$).

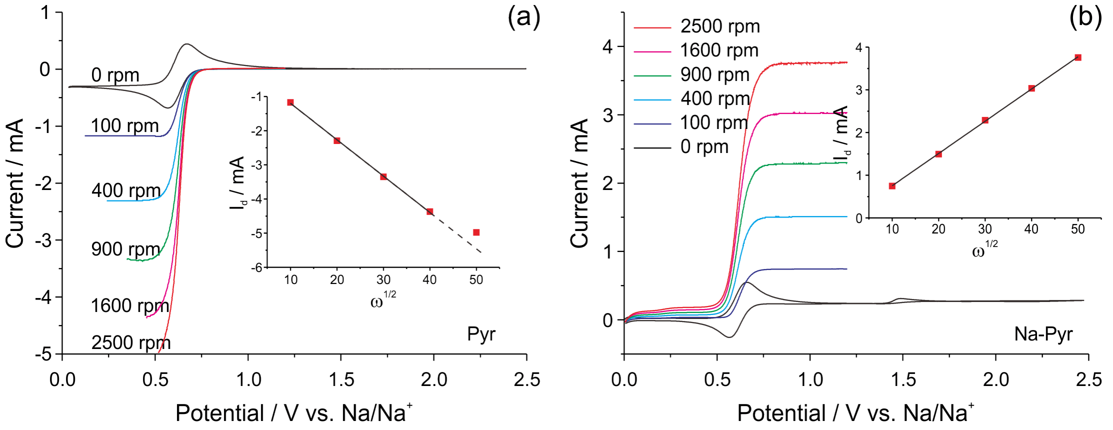

Fig. S28. *i*R-corrected LSV curves for 0.01 M Pyr (a) and 0.01 M Na-Pyr (b) contained electrolytes at various rotation speeds. Insert are the Levich plots of diffusion-limited current (i_d) vs. square root of rotation ($\omega^{1/2}$).

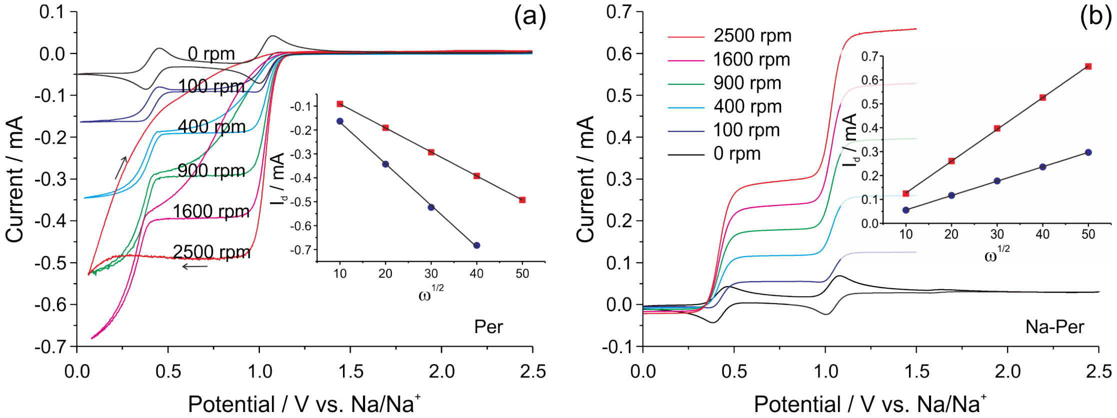

Fig. S29. *i*R-corrected LSV curves for 0.01 M Per (a) and 0.01 M Na-Per (b) contained electrolytes at various rotation speeds. Insert are the Levich plots of diffusion-limited current (i_d) vs. square root of rotation ($\omega^{1/2}$).

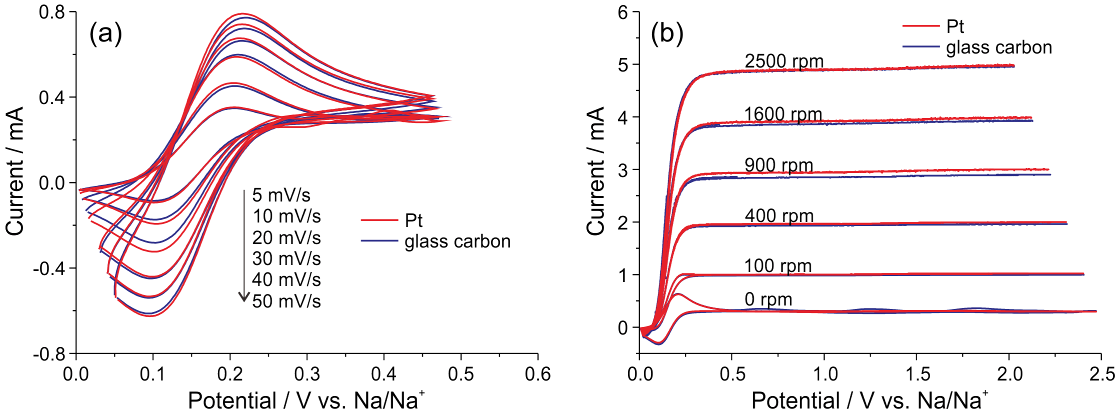

Fig. S30. *i*R-corrected CV curves of Pt and glass carbon RDE in 0.1 M Na-Nap contained electrolyte at different scan rates (a) and different rotation speeds (b)

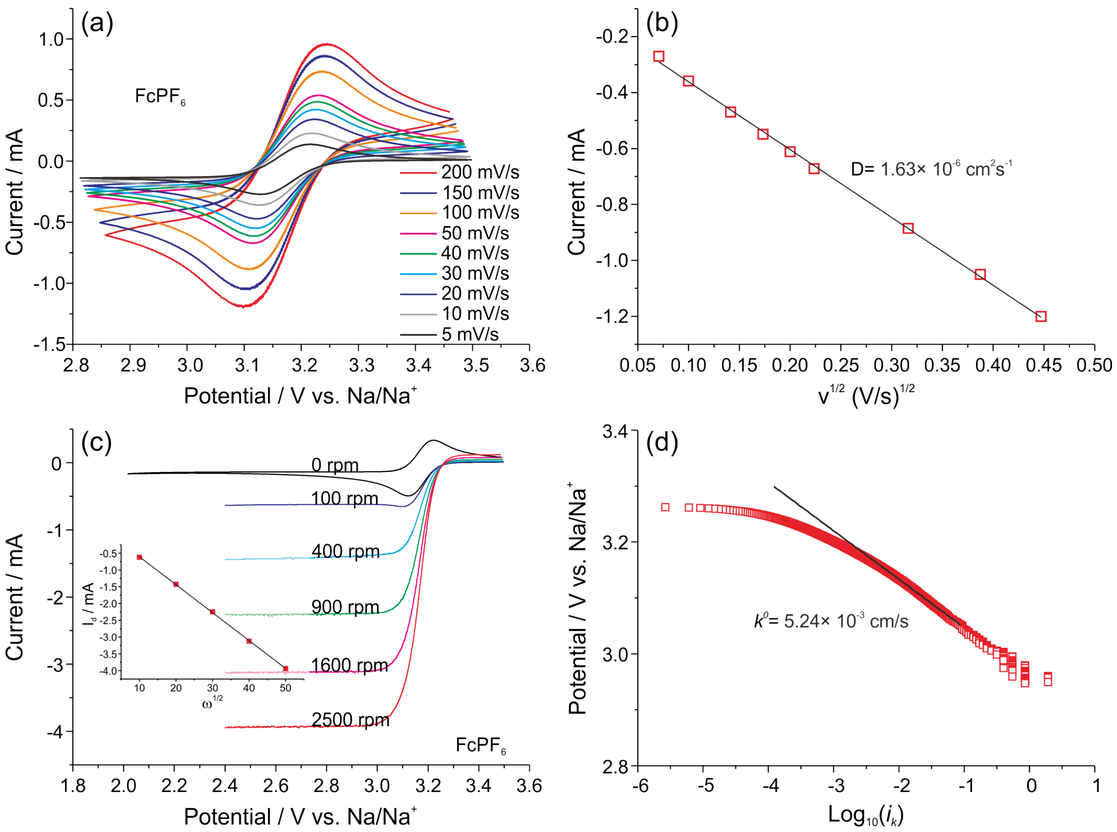

Fig. S31. *i*R-corrected CV curves for 0.1 M $FcPF_6$ contained electrolytes at different scan rates (a). Linear relationship between i_p and $v^{1/2}$ obtained from CV curves (b). *i*R-corrected LSV curves for 0.1 M $FcPF_6$ contained electrolytes at various rotation speeds (c). Insert is the Levich plot of diffusion-limited current (i_d) vs. square root of rotation ($\omega^{1/2}$). Plot of potential versus $\log_{10}(i_k)$ and the corresponding fitted Tafel plot (d).

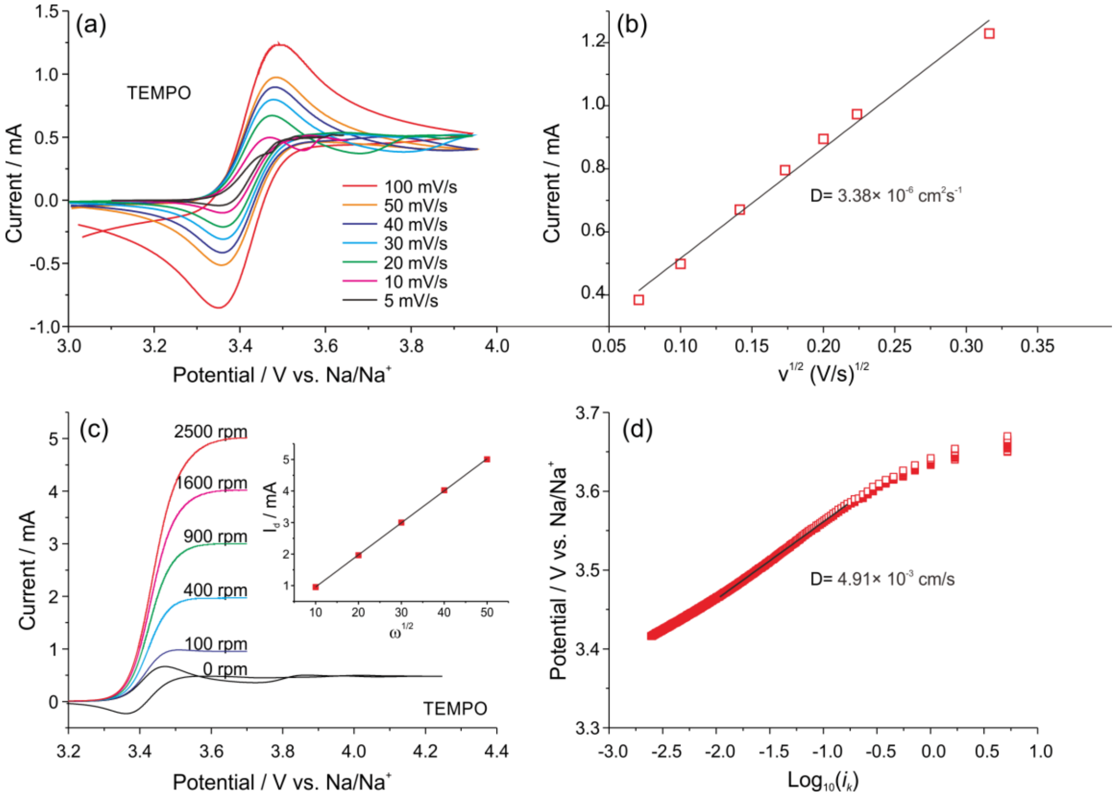

Fig. S32. *i*R-corrected CV curves for 0.1 M TEMPO contained electrolytes at different scan rates (a). Linear relationship between i_p and $v^{1/2}$ obtained from CV curves (b). *i*R-corrected LSV curves for 0.1 M TEMPO contained electrolytes at various rotation speeds (c). Insert is the Levich plot of diffusion-limited current (i_d) vs. square root of rotation ($\omega^{1/2}$). Plot of potential versus $\log_{10}(i_k)$ and the corresponding fitted Tafel plot (d).

Table S3. The rate constant (k^0, cm/s) of as-studied redox species

	k, ×10^{-3} cm/s				*k*, ×10^{-3} cm/s		
	PAH/ PAH$^{\bullet-}$	PAH$^{\bullet-}$/ PAH$^{\bullet2-}$	PAH$^{\bullet2-}$/ PAH$^{\bullet3-}$		PAH$^{\bullet-}$/ PAH	PAH$^{\bullet2-}$/ PAH$^{\bullet-}$	PAH$^{\bullet3-}$/ PAH$^{\bullet2-}$
Bp				Na-Bp	6.16		
Nap				Na-Nap	10.4		
Phe				Na-Phe	9.70		
Ant	7.97			Na-Ant	5.00	1.95	
Tet	6.05			Na-Tet	4.94	4.02	
Pyr	15.3			Na-Pyr	4.56		
Per	8.07			Na-Per	5.64	15.7	
FcPF$_6$	5.24						
				TEMPO	4.91		

5. Stability, Conductivity and Viscosity

Nap is a stable molecule. The durability of Nap/Nap$^{\bullet-}$ based anolyte depends on the stability of Nap$^{\bullet-}$. In order to evaluate the stability of Nap$^{\bullet-}$, CV was performed in 0.1 M Na-Nap contained electrolyte (ca. 0.5 ml) at a potential range of 0 ~ 0.4 V (vs. Na/Na^{+}) with a scan rate of 20 mV/s in glovebox. Both the working and counter electrodes were Pt wire, and the reference electrode was also a homemade Na/Na^{+} electrode. As shown in Fig. S33, the CVs shows negligible decay after 4000 cycles (over 40 hours), indicating a good stability of Nap$^{\bullet-}$.

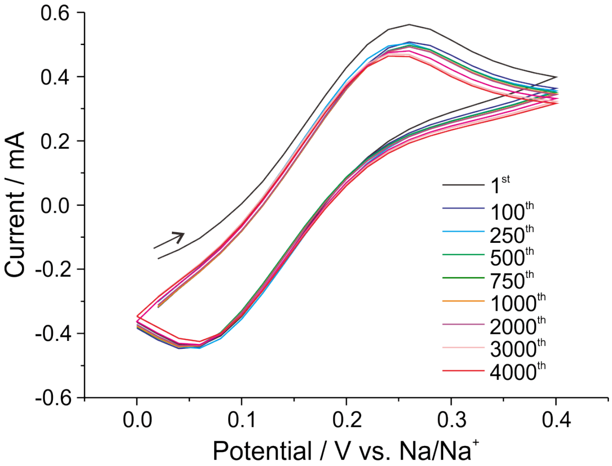

Fig. S33. CV curves for 0.1 M Na-Nap contained electrolyte after different cycles at a scan rate of 20 mV/s. Both working electrode and counter electrode are Pt wire. The CVs shows negligible decay after 4000 cycles (over 40 hours), indicating a good stability of Nap$^{\cdot-}$.

The conductivity of Nap and Na-Nap contained electrolytes with various concentrations were studied using AC impedance inside glovebox (Fig. S34). A two-electrode system was used. Both the working and counter electrodes were Ni foil (1 cm^{2}) and the distance between the two electrodes was 1 cm. the conductivity was calculated according to the following equation:

$$\rho = \frac{l}{sR}$$

where ρ is the ionic conductivity (S/cm), l is the distance of working and counter electrodes (1 cm), s is the electrode surface area (1 cm^{2}), and R is the solution resistance (Ω) which obtained from the AC impedance analysis.

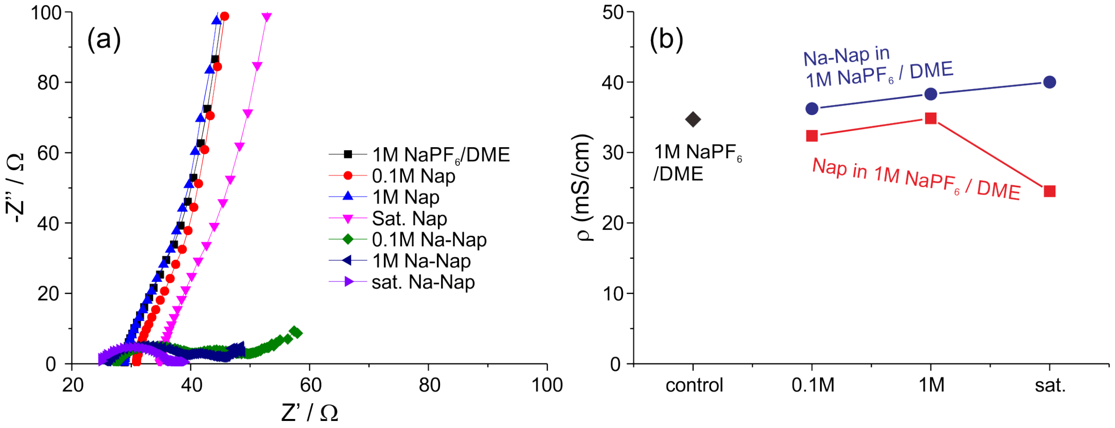

Fig. S34. Electrochemical impedance spectra (EIS) and conductivities of blank electrolyte (1 M NaPF$_6$ / DME), Nap contained electrolytes and Na-Nap contained electrolytes.

The viscosities of Nap and Na-Nap contained electrolytes with various concentrations were measured on a Brookfield DV-II+Pro viscometer under air atmosphere at room temperature (Fig. S35). Spindle SC-21 was used in this viscometer. Na-Nap saturated electrolyte would react with oxygen or moisture and formed an insoluble film on the surface, thus restricting the rotation of spindle and resulting a sharp rise of viscosity. The real viscosity for Na-Nap saturated electrolyte should be lower than the measured value.

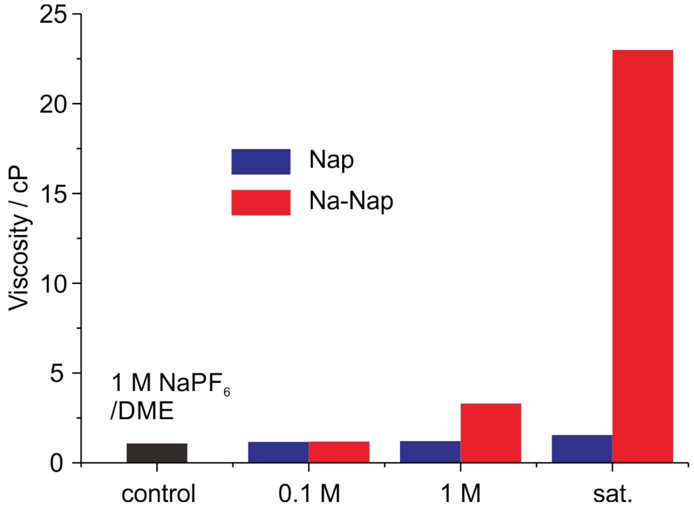

Fig. S35. The viscosities of Nap and Na-Nap contained electrolytes with various concentrations. The obtained viscosities for Nap and Na-Nap contained electrolytes were very low, which could facilitate the flow of electrolyte and mass transfer of redox-active species.

6. Battery test

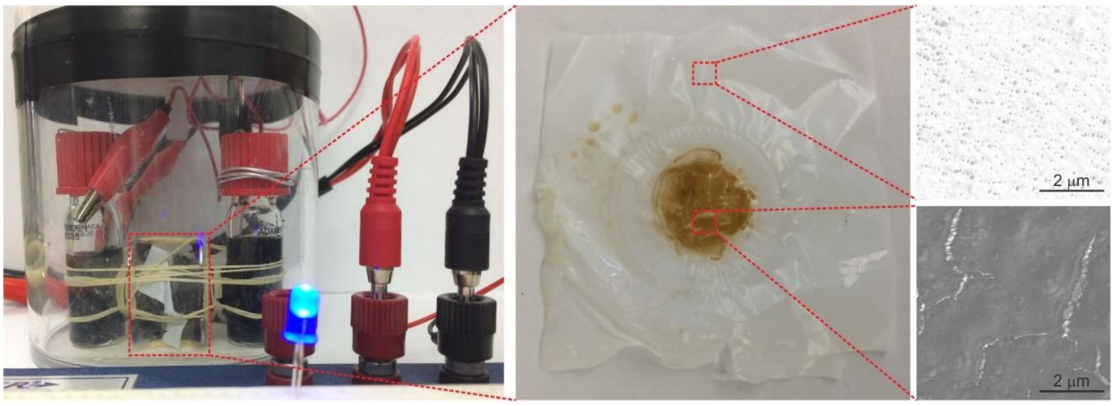

Fig. S36. H-type Na-Nap||FcPF$_6$ battery and the separator (Celgard M824) after cycling test.

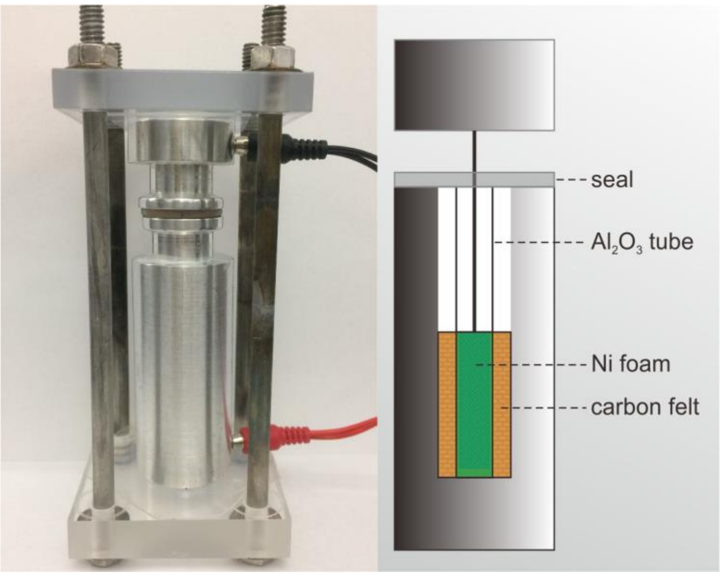

Fig. S37. Photograph and scheme of the cylinder type Nap||TEMPO battery.

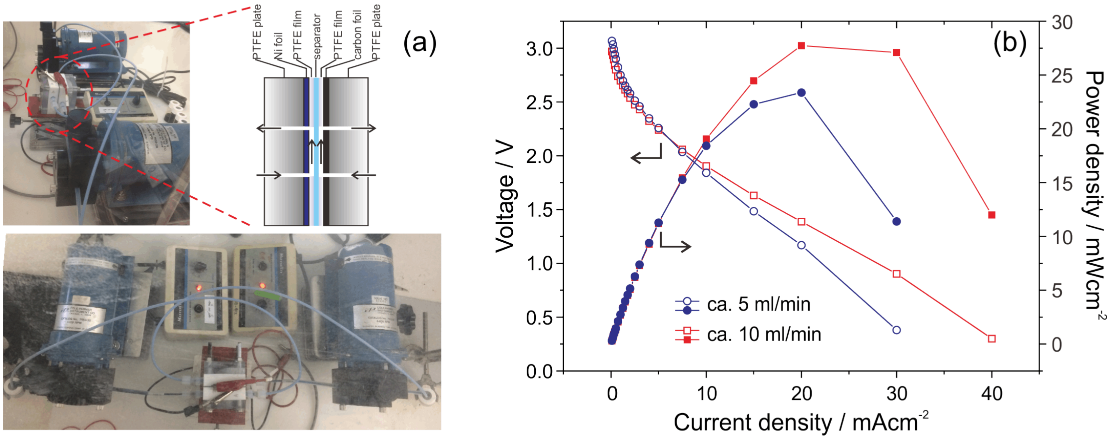

Fig. S38. Photograph and scheme of flow-mode Na-Nap||FcPF$_6$ RFB (a). Polarization curve and corresponding power density of the Na-Nap||FcPF$_6$ RFB at a flow rate of 5 ml/min and 10 ml/min, respectively (b). Anolyte is 8 ml 0.1 M Na-Nap 1 M NaPF$_6$/DME and catholyte is 8 ml 0.1 M FcPF$_6$ 1 M NaPF$_6$/DME. The separator is a Celgard M824 membrane. The polarization curves were collected by multi-step constant current method and each current step was 1 min.

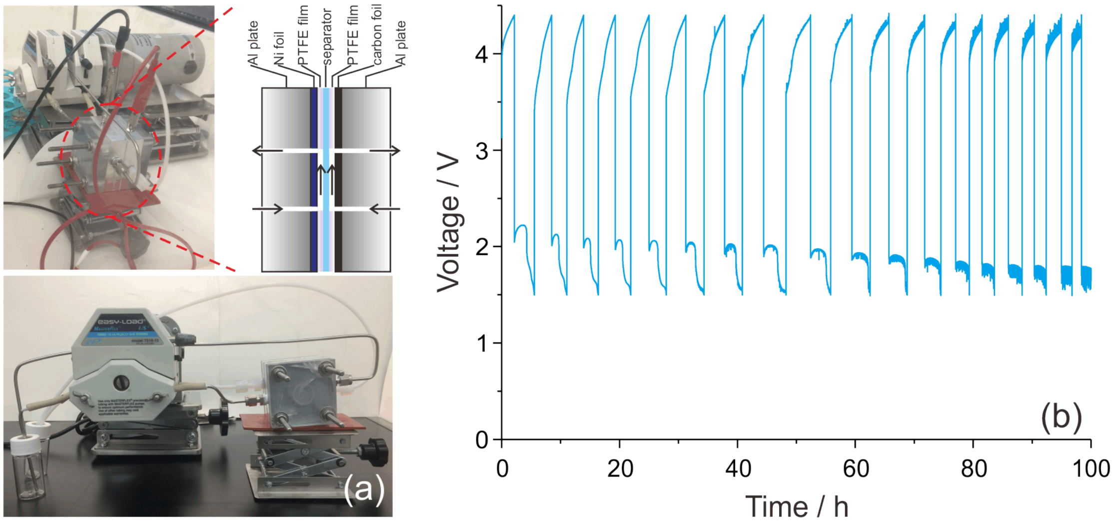

Fig. S39. Photograph and scheme of flow-mode Nap||TEMPO RFB (a). Cycling performance of the Nap||TEMPO RFB at ± 0.2 mA (b). Anolyte is 8 ml 0.1 M Nap 1 M $NaPF_6$/DME and catholyte is 8 ml 0.1 M TEMPO 1 M $NaPF_6$/DME. The separator is a Na^+ conducting beta-alumina disk (Ionotec Company).

7. A summary of reported redox species in the literatures

Table S4. A summary of redox species adopted in flow batteries. All the potentials were converted to standard hydrogen electrode (SHE) scale. In aqueous solution, the sliver – sliver chloride electrode (Ag/AgCl) and the saturated calomel electrode (SCE) are widely used. The potentials referred to Ag/AgCl and SCE can be converted to the potentials referred to SHE by relationships: E(Ag/AgCl(saturated KCl aqueous solution)) = 0.198 V vs. SHE, E(Ag/AgCl(0.1M KCl aqueous solution)) = 0.287 V vs. SHE and E(SCE) = 0.2436 V vs. SHE. In non-aqueous solution, the potentials referred to Li/Li^+, Na/Na^+, Fc/Fc^+ can be converted to the potentials referred to SHE by relationships: $E(Li/Li^+)$ = -3.04 V vs. SHE, $E(Na/Na^+)$ = -2.713 V vs. SHE and $E(Fc/Fc^+)$ = 0.45 V vs. SHE. Additionally, the Ag/Ag^+ electrode is also widely used in non-aqueous solutions. However, the $E(Ag/Ag^+)$ differ widely in different electrolytes. While the difference between the standard potential of Fc/Fc^+ redox is almost solvent-independent. Therefore, the values of $E(Ag/Ag^+)$ vs. $E(Fc/Fc^+)$ in different electrolytes were adopted to convert the potential scale (Tab 6.4 in Izutsu, Kosuke. *Electrochemistry in nonaqueous solutions.* John Wiley & Sons, 2002.)

N.	redox	E (V vs. SHE)	n	c (M)	Capacity density (Ah/L)	k^0 (cm/s)	References
1	I^{3-}/I^-	0.54	2	5	268.0		Molecules 2015, 20, 20499–20517; Nano Energy, 2016, 30, 283-292.
2	I_2Br^-/I^- and Br^-	0.594	2	5	268.0		Energy Environ. Sci., 2017, 10, 735-741
3	$ClBr_2^-/Br^-$	1.04	2	1	53.6		Molecules 2015, 20, 20499–20517; ChemsusChem 2012, 5, 867-869
4	Br_2/Br^-	1.09	2	2	107.2	0.00058	Molecules 2015, 20, 20499–20517; J. Appl. Electrochem. 2011, 41, 1137-1164; Energy Environ. Sci., 2014, 7, 1990-1995
5	Br^-/Br_3^-	1.09	2				Nat. Commun. 2016, 7, 11474
6	S/S^{2-}	-0.64	2				Adv. Energy. Mater. 2016, 6, 1502183; Chem. Mater., 2015, 27, 6765–6770.
7	S^{2-}/S_2^{2-}	-0.5	1	3.3	88.4		Nano Energy, 2016, 30, 283-292.

8	M(acac)$_n$ 1 ~ 17 molecules	-2.149~1.971					J. Mater. Chem. A, 2017, 5, 13700-13709
9	aluminum-based deep-eutectic solvent	-0.84	3	3.2	257.3		*Angew. Chem. Int. Ed. 2017, 56, 7454-7459.*
10	$[Ru(bpy)_3]^{3+}$/$[Ru(bpy)_3]^{2+}$	1.5	1			0.0034	J. Appl. Electrochem., 1988, 18, 909–914.; Bull. Chem. Soc. Jpn., 1988, 61, 2711–2714.
11	$[Ru(acac)_3]^+$/$[Ru(acac)_3]$	1.2	1	0.1	2.7	0.046	Energy Environ. Sci 2015, 8, 3515-3530; Electrochim. Acta 2007, 52, 2189–2195.
12	$[Ru(acac)_3]$/$[Ru(acac)_3]^-$	-0.5	1	0.1	2.7		Energy Environ. Sci 2015, 8, 3515-3530; Electrochim. Acta 2007, 52, 2189–2195.
13	$[Ru(bpy)_3]^{2+}$/$[Ru(bpy)_3]^+$	-1.1	1			0.2	Energy Environ. Sci 2015, 8, 3515-3530
14	Fe^{3+}/Fe^{2+}	0.77	1	2	53.6	0.000022	Molecules 2015, 20, 20499–20517; J. Appl. Electrochem. 2011, 41, 1137-1164
15	Fe^{2+}/Fe	-0.3	2				J. Appl. Electrochem. 2011, 41, 1137-1164
16	$[Fe(bpy)_3]^{3+}$/$[Fe(bpy)_3]^{2+}$	1.3	1	0.4	10.7	0.013	Energy Environ. Sci 2015, 8, 3515-3530; Electrochim. Acta 2007, 52, 2189–2195.; Molecules 2015, 20, 20499–20517; Adv. Funct. Mater. 2017, 27, 1604299
17	$[Fe(bpy)_3]^{2+}$/$[Fe(bpy)_3]^+$	-1.1	1	0.4	10.7	0.16	Energy Environ. Sci 2015, 8, 3515-3530; Electrochim. Acta 2007, 52, 2189–2195.; Molecules 2015, 20, 20499–20517
18	Fe(III)-TEOA / Fe(II)-TEOA	-0.86	1			0.011	ACS Energy Lett., 2016, 1, 89–93
19	$Fe(CN)_6^{3-}$/$Fe(CN)_6^{4-}$	0.36	1			0.25	ACS Energy Lett., 2016, 1, 89–93

20	$Fe(CN)_6^{3-}/Fe(CN)_6^{4-}$	0.5	1	0.4	10.7		Science, 2015, 349, 1529.; Energy Environ. Sci. 2014, 7,2986–2998
21	Ferrocene/Ferrocenium	0.36	1	0.6	16.1	0.1, 0.014, 0.0068	*Nano Lett.*, 2015, *15*, 4108–4113; Angew. Chem. Int. Ed. 2014, 126, 11216–11220; Angew. Chem. Int. Ed. 2014, 53, 11036-11040
22	FcNCl	0.61	1	4	107.2		J. Am. Chem. Soc. 2017, 139, 1207-1214; Angew. Chem. Int. Ed. 2017, 56, 8614-8616
23	Fc1N112-TFSI	0.45	1	0.8	21.4		Adv. Energy. Mater. 2015, 5, 1400678
24	BTMAP-Fc (bis((3-trimethylammonio)propyl)ferrocene dichloride)	0.39	1	2	53.6	0.014	*ACS Energy Lett.*, 2017, *2*, 639–644
25	$[Ni(bpy)_3]^{2+}/Ni(bpy)_3$	-1.2	2	0.2	10.7		Electrochem. Solid-State Lett. 2012, 15, A80-A82.
26	Nickelocene (Ni^{3+} / Ni^{2+})	0.287	1	0.003	0.1	0.000015	Energy Environ. Sci., 2017, 10, 491-497
27	Nickelocene (Ni^{4+} / Ni^{3+})	1.287	1	0.003	0.1		Energy Environ. Sci., 2017, 10, 491-497
28	NiCp*2 (bis-(pentamethyl-cyclopentadienyl) nickel)	-0.55	1				Adv. Energy. Mater. 2015, 5, 1501808
29	Nickel(II)-1,4,8,11-tetraazacyclotetradecane	-1.36	1	0.4	10.7		J. Power Sources 2015, 283, 300-304

30	Nickel(II)-1,4,8,11-tetraazacyclotetradecane	1.19	1	0.4	10.7		J. Power Sources 2015, 283, 300-304
31	$[Mn(acac)_3]^+/Mn(acac)_3$	1.2	1	0.05	1.3		J. Power Sources 2011, 196, 5742-5745.
32	$Mn(acac)_3/[Mn(acac)_3]$	0.1	1	0.05	1.3		J. Power Sources 2011, 196, 5742-5745.
33	MnO_4^-/MnO_4^{2-}	0.558	1	3.62	97.0		Chem. Commun., 2016, 52, 14039-14042
34	Mn^{3+}/Mn^{2+}	1.51	1	0.3	8.0		Molecules 2015, 20, 20499–20517
35	Pb^{2+}/Pb	-0.13	2				J. Appl. Electrochem. 2011, 41, 1137-1164
36	Zn^{2+}/Zn	-0.76	2				Molecules 2015, 20, 20499–20517; ChemsusChem 2012, 5, 867-869
37	V^{3+}/V^{2+}	-0.26	1	2	53.6	0.004	Molecules 2015, 20, 20499–20517; J. Appl. Electrochem. 2011, 41, 1137-1164
38	VO_2^+/VO^{2+}	1	1	2	53.6	0.0000003	Molecules 2015, 20, 20499–20517; J. Appl. Electrochem. 2011, 41, 1137-1164; Nano Energy 2016, 22, 396-405.
39	$[V(acac)_3]^+/V(acac)_3$	1	1	0.8	21.4	0.00065	Electrochim. Acta 2013, 113, 127-133.
40	$V(acac)_3/[V(acac)_3]^-$	-1.2	1	0.59	15.8	0.00087	Electrochem. Commun. 2009, 11, 2312-2315; J. Appl. Electrochem. 2011, 41, 1191-1199.
41	$[V(mnt)_3]^-/[V(mnt)_3]^{2-}$	0.9	1	0.02	0.5		Adv. Energy Mater. 2014, 4, 1300566
42	$[V(mnt)_3]^{2-}/[V(mnt)_3]^{3-}$	-0.2	1				Adv. Energy Mater. 2014, 4, 1300566
43	$[V(mnt)_3]^{3-}/[V(mnt)_3]^{4-}$	-1.4	1	0.02	0.5		Adv. Energy Mater. 2014, 4, 1300566
44	VCl_3/VCl_2	-0.34	1	1	26.8		Molecules 2015, 20, 20499–20517
45	VBr_3/VBr_2	-0.26	1	3	80.4		Molecules 2015, 20, 20499–20517

46	CVBH (calcium(II) vanadium(IV) bis-hydroxyiminodiacetate)	0.3	1	0.005	0.1		J. Mater. Chem. A, 2017, 5, 11586-11591
47	Cr^{3+}/Cr^{2+}	-0.41	1	1	26.8	0.0002	Molecules 2015, 20, 20499–20517; J. Appl. Electrochem. 2011, 41, 1137-1164
48	CrCp*2 (bis-(pentamethyl-cyclopentadienyl) chromium)	-1.08	1				Adv. Energy. Mater. 2015, 5, 1501808
49	$[Cr(acac)_3]^+/Cr(acac)_3$	1	1	0.4	10.7		Electrochem. Commun. 2010, 12, 1634-1637.
50	$Cr(acac)_3/[Cr(acac)_3]^-$	-1.8	1	0.4	10.7		Electrochem. Commun. 2010, 12, 1634-1637.
51	$[Co(acacen)]^+$/Co(acacen)	0.3	1	0.01	0.3		J. Power Sources 2012, 217, 199-203.
52	Co(acacen)/$[Co(acacen)]^-$	-1.7	1	0.01	0.3		J. Power Sources 2012, 217, 199-203.
53	Cobaltocene (Co2+/Co1+)	-1.24	1	1	26.8	0.00053	Energy Environ. Sci., 2017, 10, 491-497
54	Cobaltocene (Co3+/Co2+)	-0.66	1	1	26.8		Energy Environ. Sci., 2017, 10, 491-497
55	$[Co^{II}W_{12}O_{40}]^{6-}$ / $[Co^{III}W_{12}O_{40}]^{5-}$	1.103	1				Adv. Energy. Mater. 2017, 7, 1601224
56	$[CoW_{12}O_{40}]^{6-}$ / $H_2CoW_{12}O_{40}{}^{6-}$	-0.074	2	0.8	42.9		Adv. Energy. Mater. 2017, 7, 1601224

57	$H_2CoW_{12}O_{40}^{6-}$ / $H_4CoW_{12}O_{40}^{6-}$	-0.191	2	0.8	42.9		Adv. Energy. Mater. 2017, 7, 1601224
58	Ce^{4+}/Ce^{3+}	1.75	1			0.0016	J. Appl. Electrochem. 2011, 41, 1137-1164; J. Mater. Chem. A, 2017, 5, 5036-5043
59	Ce^{3+}/Ce^{2+}	1.67	1	0.5	13.4		Molecules 2015, 20, 20499–20517
60	Ti^{4+}/Ti^{3+}	0.04	1	1.1	29.5		Molecules 2015, 20, 20499–20517
61	$[UO_2(dmso)_5]^-$ $/[UO_2(dmso)_5]^{2-}$	-0.3	1	0.8	21.4		Electrochim. Acta 2002, 48, 43-50.
62	$[UO_2(hfa)_2]^-$ $/[UO_2(hfa)_2]^{2-}$	-0.3	1	0.4	10.7		Electrochim. Acta 2002, 48, 43-50.
63	$[UO_2(tfa)_2]^-$ $/[UO_2(tfa)_2]^{2-}$	-0.3	1				Electrochim. Acta 2002, 48, 43-50.
64	$[UO_2(fod)_2]^-$ $/[UO_2(fod)_2]^{2-}$	-0.5	1				Electrochim. Acta 2002, 48, 43-50.
65	$[UO_2(pta)_2]^-$ $/[UO_2(pta)_2]^{2-}$	-0.5	1				Electrochim. Acta 2002, 48, 43-50.
66	$[UO_2(ba)_2]^-$ $/[UO_2(ba)_2]^{2-}$	-0.7	1				Electrochim. Acta 2002, 48, 43-50.
67	$UO_2(acac)_2$ $/[UO_2(acac)_2]^-$	-0.8	1			0.0077	J. Alloy Compd. 2006, 408, 1296-1301.
68	$[UO_2(dpm)_2]^-$ $/[UO_2(dpm)_2]^{2-}$	-0.8	1				Electrochim. Acta 2002, 48, 43-50.
69	$UO_2(btk)$ $/[UO_2(btk)]^-$	-0.8	1			0.00103	J. Alloy Compd. 2006, 408, 1296-1301.
70	$UO_2(etk)$ $/[UO_2(etk)]^-$	-0.8	1			0.011	J. Phys. Chem. C 2007, 111, 18812-18820.

71	$[U(tmma)_4]^{4+}/[U(tmma)_4]^{3+}$	-0.4	1			0.00000048	J. Alloy Compd. 2006, 418, 139-144.
72	$U(pta)_4/[U(pta)_4]^-$ (or $U(pta)_3$)	-1.3	1	0.4	10.7		Electrochim. Acta 2002, 48, 43-50.
73	$U(btk)_2$ /$[U(btk)_2]^-$	-1.8	1			0.0088	J. Phys. Chem. C 2007, 111, 18812-18820.
74	$U(acac)_4$ /$[U(acac)_4]^-$ (or $U(acac)_3$)	-1.8	1			0.017	J. Phys. Chem. C 2007, 111, 18812-18820.
75	$U(etk)_2$ /$[U(etk)_2]^-$	-1.8	1			0.015	J. Phys. Chem. C 2007, 111, 18812-18820.
76	$[SiV_3W_9O_{40}]^{7-}$ /$[SiV_3W_9O_{40}]^{10-}$	-0.5	3	0.45	36.2		J. Power Sources 2013, 236, 259-264.
77	$[SiV_3W_9O_{40}]^{10-}$ /$[SiV_3W_9O_{40}]^{13-}$	-2.2	3	0.45	36.2		J. Power Sources 2013, 236, 259-264.
78	Na-BP-DME	-2.623	1	5	134.0		*Nat. Commun. 2017, 8, 14629*
79	Rubrene$^{\bullet+}$/Rubrene	1.4	1				J. Chem. Soc. Pak., 2007, 29, 294–300
80	Rubrene/Rubrene$^{\bullet-}$	-0.9	1				J. Chem. Soc. Pak., 2007, 29, 294–300
81	DBBB$^{\bullet+}$/DBBB	1	1	0.4	10.7		*Adv. Energy Mater. 2012,* 2, 1390-1396.; Adv. Energy Mater. 2015, 5, 1401782
82	ANL-8, ANL-9, ANL-10	1	1	liquid			*Adv. Energy Mater. 2015, 5, 1401782*
83	DBMMB / DBMMB$^{\bullet-}$	1.091	1			0.0135	Angew. Chem. Int. Ed. 2015, 54, 8684–8687; ACS Energy Lett., 2016, 1, 705–711
84	TDT (1,2,3,4-tetrahydro-6,7-dimethoxy-1,1,4,4-	1.17	1	1	26.8		*Chem. Mater.*, 2016, *28*, 2529–2539

	tetramethylnaphthalene)						
85	TEMPO+/TEMPO$^{\bullet}$	0.9	1			0.1	Electrochem. Solid-State Lett. 2011, 14, A171-A173.; Adv. Mater. 2014, 26, 7649-7653
86	TEMPO-4-sulfate potassium salt	0.892	1	1	26.8	0.00191	*ACS Energy Lett.*, 2017, *2*, 411–416
87	4-HO-TEMPO	0.8	1	2.1	56.3	0.00026	Adv. Energy Mater. 2016, 6, 1501449
88	TEMPTMA	1.077	1	3.2	85.8	0.0042	Angew. Chem. Int. Ed. 2016, 55, 14427–14430
89	TEMPO polymer	0.99					Nature 2015, 527, 78-81
90	Quinoxaline/Quinoxaline$^{\bullet -}$	0.1	1				*Adv. Energy Mater. 2012,* 2, 1390-1396.
91	Quinoxaline$^{\bullet -}$/Quinoxaline$^{\bullet 2-}$	-0.4	1				*Adv. Energy Mater. 2012,* 2, 1390-1396.
92	DPh-quinoxaline/DPh-quinoxaline$^{\bullet -}$	0	1				*Adv. Energy Mater. 2012,* 2, 1390-1396.
93	Me-quinoxaline/Me-quinoxaline$^{\bullet -}$	-0.1	1				*Adv. Energy Mater. 2012,* 2, 1390-1396.
94	DMe-quinoxaline/DMe-quinoxaline$^{\bullet -}$	-0.2	1				*Adv. Energy Mater. 2012,* 2, 1390-1396.
95	DMe-quinoxaline$^{\bullet -}$/DMe-quinoxaline$^{\bullet 2-}$	-0.5	1				*Adv. Energy Mater. 2012,* 2, 1390-1396.
96	TMe-quinoxaline/TMe-quinoxaline$^{\bullet -}$	-0.2	1				*Adv. Energy Mater. 2012,* 2, 1390-1396.

97	TMe-quinoxaline$^{\bullet-}$ /TMe-quinoxaline$^{\bullet 2-}$	-0.5	1				*Adv. Energy Mater. 2012,* 2, 1390-1396.
98	DPh-quinoxaline$^{\bullet-}$ /DPh-quinoxaline$^{\bullet 2-}$	-0.3	1				*Adv. Energy Mater. 2012,* 2, 1390-1396.
99	Me-quinoxaline$^{\bullet-}$/Me-quinoxaline$^{\bullet 2-}$	-0.4	1				*Adv. Energy Mater. 2012,* 2, 1390-1396.
100	acylpyridinium derivative 1^+ / 1	-1.63	1	1.5	40.2		*J. Am. Chem. Soc.*, 2017, *139*, 2924–2927
101	acylpyridinium derivative 1^- / 1	-1.93	1	1.5	40.2		*J. Am. Chem. Soc.*, 2017, *139*, 2924–2927
102	*N*-methyl 4-acetylpyridinium tetrafluoroborate	-0.639	1	1.6	42.9		J. Am. Chem. Soc., 2015, 137, 14465–14472
103	*N*-methyl 4-acetylpyridinium tetrafluoroborate	-1.039	1	0.062	1.7		J. Am. Chem. Soc., 2015, 137, 14465–14472
104	phenazine derivative	-0.313	1	0.01	0.3		*ACS Energy Lett.*, 2016, *1*, 976–980
105	BzNSN	-1.219	1	0.5	13.4	0.009	*ACS Energy Lett.*, 2017, *2*, 1156–1161.
106	FMN^{3-} / FMN^{5-}	-0.85	2	0.01	0.5	0.0053	Nat. Commun. 2016, 7, 13230
107	MV	-0.343	1	2.5	67.0	0.0033	Angew. Chem. Int. Ed. 2016, 55, 14427–14430
108	MV	-0.45	1	3.5	93.8		J. Am. Chem. Soc. 2017, 139, 1207-1214; Angew. Chem. Int. Ed. 2017, 56, 8614-8616
109	MV^{2+} / MV^+	-0.45	1	3	80.4	0.00028	Adv. Energy Mater. 2016, 6, 1501449
110	viologen monomer 2	-0.359	1				Chem. Mater., 2016, 28, 7362–7374.
111	viologen monomer 2	-0.799	1				Chem. Mater., 2016, 28, 7362–7374.
112	viologen dimer 3	-0.279	1				Chem. Mater., 2016, 28, 7362–7374.

113	viologen dimer 3	-0.829	1				Chem. Mater., 2016, 28, 7362–7374.
114	viologen dimer 4	-0.339	1				Chem. Mater., 2016, 28, 7362–7374.
115	viologen dimer 4	-0.799	1				Chem. Mater., 2016, 28, 7362–7374.
116	viologen dimer 5	-0.349	1				Chem. Mater., 2016, 28, 7362–7374.
117	viologen dimer 5	-0.799	1				Chem. Mater., 2016, 28, 7362–7374.
118	viologen dimer 6	-0.354	1				Chem. Mater., 2016, 28, 7362–7374.
119	viologen dimer 6	-0.799	1				Chem. Mater., 2016, 28, 7362–7374.
120	viologen dimer 7	-0.359	1				Chem. Mater., 2016, 28, 7362–7374.
121	viologen dimer 7	-0.799	1				Chem. Mater., 2016, 28, 7362–7374.
122	viologen o-benzene dimer 8	-0.309	1				Chem. Mater., 2016, 28, 7362–7374.
123	viologen o-benzene dimer 8	-0.869	1				Chem. Mater., 2016, 28, 7362–7374.
124	viologen m-benzene dimer 9	-0.359	1				Chem. Mater., 2016, 28, 7362–7374.
125	viologen m-benzene dimer 9	-0.799	1				Chem. Mater., 2016, 28, 7362–7374.
126	viologen poly o-benzene dimer 10	-0.279	1				Chem. Mater., 2016, 28, 7362–7374.
127	viologen poly o-benzene dimer 10	-0.839	1				Chem. Mater., 2016, 28, 7362–7374.
128	viologen poly m-benzene dimer 11	-0.319	1				Chem. Mater., 2016, 28, 7362–7374.
129	viologen poly m-benzene dimer 11	-0.839	1				Chem. Mater., 2016, 28, 7362–7374.

130	poly benzene monoviologen 1	-0.329	1				Chem. Mater., 2016, 28, 7362–7374.
131	poly benzene monoviologen 1	-0.799	1				Chem. Mater., 2016, 28, 7362–7374.
132	viologen-containing polymer	-0.113	1				Nature 2015, 527, 78-81
133	viologen-containing polymer	-0.513	1				Nature 2015, 527, 78-81
134	Viologen-based redox active colloids	-0.339	1	0.56	15.0	0.015	*J. Am. Chem. Soc.*, 2016, *138*, 13230–13237.
135	Viologen-based redox active colloids	-0.939	1	0.56	15.0		*J. Am. Chem. Soc.*, 2016, *138*, 13230–13237.
136	Viologen RAPs1~5	-0.339	1				*J. Am. Chem. Soc.*, 2014, *136,* 16309–16316
137	Viologen RAPs1~5	-0.839	1				*J. Am. Chem. Soc.*, 2014, *136,* 16309–16316
138	EV^0/EV^+ (ethyl viologen diiodide)	-0.99	1				*ACS Energy Lett.*, 2017, *2*, 615–621
139	EV^+/EV^{2+} (ethyl viologen diiodide)	-0.59	1				*ACS Energy Lett.*, 2017, *2*, 615–621
140	BTMAP-Vi (bis(3-trimethylammonio)propyl viologen tetrachloride)	-0.358	1	2	53.6	0.022	*ACS Energy Lett.*, 2017, *2*, 639–644
141	BODIPY (boron-dipyrromethene)	0.34		13mg/ml			*Chem. Mater.*, 2016, *28*, 3401–3405
142	BODIPY (boron-dipyrromethene)	-1.14		13mg/ml			*Chem. Mater.*, 2016, *28*, 3401–3405

143	M(L5)2	-1.339	2	0.71	38.1		*J. Am. Chem. Soc.*, 2016, *138*, 15378–15384
144	M(L5)2	-1.539	2	0.71	38.1		*J. Am. Chem. Soc.*, 2016, *138*, 15378–15384
145	2,6-DHAQ / 2,6-reDHAQ	-0.69	2	0.5	26.8		Science, 2015, 349, 1529.
146	$15D3GAQ^{\bullet -}$ /$15D3GAQ^{2-}$	-0.5	1	0.25	6.7		*Chem. Commun., 2012, 48, 6669–6671*
147	$15D3GAQ/15D3GAQ^{\bullet -}$	-0.8	1	0.25	6.7		*Chem. Commun., 2012, 48, 6669–6671*
148	AQDS	0.21	2	1	53.6	0.0105	*Adv. Energy Mater. 2017, 7, 1601488; Chem. Mater., 2017, 29, 4801–4810; Nat. Commun. 2016, 7, 11474; Nature 2014, 505, 195-198*
149	AQDS (anthraquinone-2,7-disulphonate)	-0.25	2	0.1	5.4		Angew. Chem. Int. Ed. 2016, 55, 7142–7147.
150	AQS	0.187	2	2	107.2		*Adv. Energy Mater. 2017, 7, 1601488*
151	DHAQDS	0.12	2	1	53.6		*Adv. Energy Mater. 2017, 7, 1601488*
152	ARS	0.082	2				*Adv. Energy Mater. 2017, 7, 1601488*
153	DHAQDMS	0.02	2	1	53.6		*Adv. Energy Mater. 2017, 7, 1601488*
154	AQDSH2 / AQDS	0.21	2	0.1	5.4		Angew. Chem. Int. Ed. 2016, 55, 13104–13108
155	BQDS	0.89	2	0.1	5.4		Angew. Chem. Int. Ed. 2016, 55, 13104–13108
156	FL / $FL^{\bullet -}$ (9-fluorenone)	-1.279	1	2	53.6		Angew. Chem. Int. Ed. 2015, 54, 8684–8687
157	PTIO / $PTIO^{-}$	-0.91	1	2.6	69.7		J. Mater. Chem. A, 2016, 4, 5448-5456
158	PTIO / $PTIO^{+}$	0.82	1	2.6	69.7		J. Mater. Chem. A, 2016, 4, 5448-5456

159	$NMPI/NMPI^{\bullet -}$	potential=-1.30 vs. Ag wire	1	0.1	2.7	0.046	Electrochem. Solid-State Lett. 2011, 14, A171-A173.
160	$MePh$ / $MePh^{\bullet -}$	-1.429	1	0.3	8.0	0.00246	*ACS Energy Lett.*, 2016, 1, 705–711
161	hydroquinone	0.65	2	1	53.6	0.002	*Angew. Chem. Int. Ed. 2016, 55, 4772-4776*
162	NAQ (5,12-naphthacenequinone)	-0.84	2	0.05	2.7		Adv. Mater. 2015, 27, 5141-5146
163	BAQ (1,2-benzanthraquinone)	-0.74	2	0.5	26.8		Adv. Mater. 2015, 27, 5141-5146
164	BAQ (1,2-benzanthraquinone)	-0.54	2	0.5	26.8		Adv. Mater. 2015, 27, 5141-5146
165	quinizarin	-0.037	2	1.6	85.8		Energy Environ. Sci., 2016, 9, 3521-3530
166	quinizarin	1.087	2	1.6	85.8		Energy Environ. Sci., 2016, 9, 3521-3530
167	EPT	0.72	1	2	53.6		Energy Environ. Sci., 2016, 9, 3531-3543
168	MEPT	0.76	1	2	53.6		Energy Environ. Sci., 2016, 9, 3531-3543
169	MEEPT	0.76	1	2	53.6		Energy Environ. Sci., 2016, 9, 3531-3543
170	$TMPD/TMPD^{\bullet +}$	0.16	1				J. Am. Chem. Soc., 2017, 139, 6286–6289
171	$TMPD^{\bullet +}$/ $TMPD^{\bullet 2+}$	0.56	1				J. Am. Chem. Soc., 2017, 139, 6286–6289
172	cyclopropenium derivatives	1.25	1	0.7	18.8		*Adv. Energy. Mater. 2017,7, 1602027*
	Bp / Bp^{-}	-2.618	1	3.9	104.5	0.00616	This work
	Nap / Nap^{-}	-2.559	1	4	107.2	0.0104	This work
	Phe / Phe^{-}	-2.489	1	3.15	84.4	0.0097	This work
	Ant^{-} / Ant^{2-}	-2.570	1	0.093	2.5	0.00195	This work
	Ant / Ant^{-}	-1.988	1	0.093	2.5	0.005	This work

	Tet^{2-} / Tet^{3-}	-2.590	1	0.0022	0.1		This work
	Tet^{-} / Tet^{2-}	-2.205	1	0.0022	0.1	0.00402	This work
	Tet / Tet^{-}	-1.595	1	0.0022	0.1	0.00494	This work
	Pyr / Pyr^{-}	-2.101	1	1.26	33.8	0.00456	This work
	Per^{-} / Per^{2-}	-2.295	1	0.016	0.4	0.0157	This work
	Per / Per^{-}	-1.679	1	0.016	0.4	0.00564	This work